CELL BIOLOGY

Discoveries of GPR39 as an evolutionarily conserved receptor for bile acids and of its involvement in biliary acute pancreatitis

Zhentao Zi[1,2] and Yi Rao[1,2,3]*

Acute pancreatitis (AP) is one of the most common gastrointestinal diseases. Bile acids (BAs) were proposed to be a cause of AP nearly 170 years ago, though the underlying mechanisms remain unclear. Here, we report that two G protein–coupled receptors, GPR39 and GHSR, mediated cellular responses to BAs. Our results revealed GPR39 as an evolutionarily conserved receptor for BAs, particularly 3-O-sulfated lithocholic acids. In cultured cell lines, GPR39 is sufficient for BA-induced Ca^{2+} elevation. In pancreatic acinar cells, GPR39 mediated BA-induced Ca^{2+} elevation and necrosis. Furthermore, AP induced by BAs was significantly reduced in GPR39 knockout mice. Our findings provide in vitro and in vivo evidence demonstrating that GPR39 is necessary and sufficient to mediate BA signaling, highlighting its involvement in biliary AP pathogenesis, and suggesting it as a promising therapeutic target for biliary AP.

INTRODUCTION

Acute pancreatitis (AP) is one of the top two reasons for gastrointestinal hospitalization (*1*), and gallstones are the most common etiology of AP (*2*). Experiments with dogs by the great French physiologist Claude Bernard first hinted at the possibility of bile induction of pancreatitis (*3*). Observations in patients supported the idea that bile reflux into the pancreas could be the cause of AP (*4*, *5*). In Opie's common channel hypothesis, gallstones at the papilla of Vater obstruct bile excretion into the duodenum, causing bile reflux into the pancreas leading to AP (*4*, *6*, *7*). More support for the bile reflux hypothesis has been obtained over the years (*8*–*11*), and it remains a predominant hypothesis today (*1*, *12*). AP is presently thought to be initiated by injuries of acinar cells (*13*, *14*), a group of exocrine cells in the pancreas susceptible to pathological stimuli, and biliary AP is thought to be caused by bile acids (BAs) (*13*, *15*–*17*).

BAs, the major organic components in the bile, are amphipathic steroids synthesized from cholesterol in the liver. After being discharged into the intestines, primary BAs are further metabolized into secondary BAs by the gut microbiota (*18*). Because of their detergent properties, BAs in the intestinal tract facilitate the digestion and absorption of fat-soluble nutrients, such as lipid and lipophilic vitamins (*19*). However, the traditional view of BAs functioning purely by their physicochemical properties as surfactants encapsulating nutrients and facilitating their absorption has been challenged (*20*–*25*). BAs have been proposed to be biologically active signals or hormones after they were found to activate either nuclear receptors (*21*–*23*, *26*) or G protein–coupled receptors (GPCRs) on the cell membrane (*24*, *25*). Specific BAs may act as hormones to regulate multiple metabolic pathways via GPCRs and/or nuclear receptors (*18*, *27*–*29*). BA signaling through receptors has implications for the treatment of diseases such as diabetes (*30*) or nonalcoholic steatohepatitis (*31*).

BAs can directly injure pancreatic acinar cells, in a Ca^{2+}-dependent manner (*14*, *32*). Taurolithocholic acid 3-sulfate (TLCAS) is a natural 3-O-sulfated and amidated secondary BA derived from lithocholic acid (LCA), which was first identified by thin-layer chromatography in 1967 (*33*). In acinar cells, TLCAS can cause elevation of cytoplasmic Ca^{2+} (*34*–*36*), secretion of amylase (*37*), depolarization of plasma membrane potential (*38*), activation of zymogen (*15*, *37*), dysfunction of mitochondria (*39*), cell injury, and death (*15*, *16*, *40*). TLCAS at a low concentration triggered Ca^{2+} elevations in isolated acini, while TLCAS at higher levels induced sustained Ca^{2+} transients which are thought to be involved in AP pathogenesis (*34*, *37*). The implication of TLCAS in AP pathogenesis highlights the significance of finding its receptor in pancreatic acinar cells.

GPCRs are the largest family of transmembrane receptors involved in cellular communications. GPCRs are the most preferred drug targets, with approximately 130 GPCRs as the targets of ~35% of drugs approved by the U.S. Food and Drug Administration and more than 300 additional drugs currently in clinical trials (*41*). There are still more than 100 GPCRs without ligands (*42*, *43*). These "orphan" GPCRs are widely expressed throughout the human body (*44*, *45*) and account for ~17% of all non-sensory GPCRs (*46*). Identifying ligands for GPCRs is important for understanding physiology, uncovering pathology, and discovering drugs (*47*–*49*).

GPR39 is one of the $G_{\alpha q}$-coupled GPCRs, belonging to the ghrelin receptor subfamily (*50*). GPR39 is highly expressed in the gastrointestinal tracts, the liver, and the pancreas (*51*, *52*) and is involved in regulating gastrointestinal motility, cholesterol metabolism (*52*), epithelial integrity (*53*), and neovascularization (*54*). GPR39 was reported to be activated by zinc (Zn^{2+}) (*55*–*57*) though it was unclear whether there are other endogenous ligands for GPR39.

We now present evidence that GPR39 is a receptor for BAs, especially for 3-O-sulfated lithocholic acids, and that GPR39 is the membrane receptor for TLCAS in pancreatic acinar cells. Genetic deletion of the gene encoding GPR39 in mice ameliorated pancreatic injuries in BA-induced AP. Our results also show that GPR39 ortholog in fish and its mammalian paralog GHSR responded to BAs but not to Zn^{2+}, suggesting that GPR39 evolutionarily first responded to BAs before

[1]Chinese Institutes for Medical Research, Beijing (CIMR, Beijing) and the State Key Laboratory of Digestive Health, Beijing Friendship Hospital, Capital Medical University, Beijing, China. [2]Peking-Tsinghua Center for Life Sciences, PKU-IDG/McGovern Institute for Brain Research, School of Life Sciences, School of Pharmaceutical Sciences, Department of Chemical Biology, College of Chemistry and Molecular Engineering, Peking University, Beijing, China. [3]Changping Laboratory, Chinese Institute of Brain Research Beijing and Research Unit of Medical Neurobiology, Chinese Academy of Medical Sciences, Beijing 102206, China.
*Corresponding author. Email: yrao@pku.edu.cn

its mammalian version responded also to Zn^{2+}. We have therefore found receptors for BAs, established an important role for GPR39, and suggested a target for the potential treatment of biliary AP.

RESULTS

GPR39 activation by taurolithocholic acid 3-sulfate

The elevated intracellular Ca^{2+} induced by TLCAS in pancreatic acinar cells was from the endoplasmic reticulum and depended on inositol trisphosphate receptors (IP3Rs) (*34*, *36*). Treatment of acinar cells with a $G_{\alpha q}$ inhibitor YM254890 (*58*) eliminated Ca^{2+} elevation induced by TLCAS (Fig. 1, A to C), indicating that the effect of TLCAS was $G_{\alpha q}$-dependent.

As illustrated in Fig. 1D, to identify the GPCRs mediating the intracellular response of Ca^{2+} elevation to TLCAS in pancreatic acinar cells, we analyzed the single-cell RNA sequencing (RNA-seq) dataset (ArrayExpress, E-MTAB-5061) of the human pancreas (*59*), from which we obtained a list of highly expressed orphan GPCRs with fragments per kilobase of transcripts per million (FPKM) larger than 1 in acinar cells and found 20 orphan GPCRs (fig. S1). To investigate whether any of these GPCRs could mediate cellular responses to TLCAS, we transfected cDNAs encoding each of the 20 human GPCRs into human embryonic kidney (HEK) 293 T cells expressing $G_{\alpha 15}$ and GCaMP6s. Cellular responses to 200 μM TLCAS were examined by confocal microscopic imaging of intracellular Ca^{2+} concentration. We found that HEK293T cells transfected with GPR39 responded robustly to TLCAS (Fig. 1E).

GPR39 was previously reported to be a Zn^{2+} receptor (*55*–*57*). We used Ca^{2+} imaging to compare the cellular response to TLCAS with that to Zn^{2+}. GPR39-expressing cells exhibited Ca^{2+} responses to 200 μM TLCAS and 200 μM Zn^{2+} (Fig. 1F), whereas mock-transfected HEK293T cells responded to neither TLCAS nor Zn^{2+} (Fig. 1G). The response to TLCAS lasted longer than that to Zn^{2+} (Fig. 1F).

We constructed HEK293T cell lines stably expressing the mouse GPR39 receptor (if not specially indicated, hereafter we used the mouse GPR39). GPR39 was activated by TLCAS in a dose-dependent manner (Fig. 1, H and J). Previous studies have demonstrated that Zn^{2+} has a positive allosteric effect on the activation of GPR39 by synthetic exogenous agonists (*60*, *61*). We examined the effect of Zn^{2+} on GPR39 activation by TLCAS. Our results showed that Zn^{2+} potentiated the GPR39-mediated calcium response to TLCAS, as shown by a leftward shift of the dose-response curve in the presence of 4 μM Zn^{2+} (Fig. 1, I and J).

Specific BAs as GPR39 agonists

BAs share a similar molecular backbone (Fig. 2A). To investigate GPR39 activation by different BAs, we examined 30 BAs (Fig. 2B), covering the major primary and secondary BAs such as cholic acid (CA), chenodeoxycholic acid (CDCA), ursodeoxycholic acid (UDCA), deoxycholic acid (DCA) and LCA, as well as their sulfated and/or amidated derivatives.

In the absence of Zn^{2+}, three 3-O-sulfated LCAs, TLCAS, glycolithocholic acid 3-sulfate (GLCAS), and lithocholic acid 3-sulfate (LCAS), activated GPR39 notably (Fig. 2, B and G, and fig. S2A), with LCAS being the most potent (Fig. 2, C and G). To a lesser extent, taurolithocholic acid (TLCA), tauro/glyco-DCA (T/G-DCA), and tauro/glyco-chenodeoxycholic acid (T/G-CDCA) could also activate GPR39 in the absence of Zn^{2+} (Fig. 2, B and H, and fig. S2A). In the presence of 4 μM Zn^{2+}, all of the tested BAs, except LCA, could activate GPR39 (Fig. 2B and fig. S2A). LCAS, TLCAS, and GLCAS were still the most efficacious BAs in the presence of Zn^{2+}, while BAs derived from CA were less potent (Fig. 2, G to L). Human GPR39 receptor (fig. S3) shows a BA profile of activation similar to that of the mouse GPR39 receptor (Fig. 2B). Although similar in structure to 3-O-sulfated LCAs, cholesterol (Fig. 2F), cholesterol-S (Fig. 2, D and F), and cholic acid 7-sulfate (CA7S) (Fig. 2, E and F) could not activate GPR39, even in the presence of 4 μM Zn^{2+}. Although there was a report for GPR39 activation by 15(S)-hydroxyeicosatetraenoic acid (HETE) and blocked by 14(15)-epoxyeicosatrienoic acid (EET) recently (*62*), we observed neither 15(S)-HETE activation nor 14(15)-EET blockade of GPR39 (fig. S2, C and D).

GPBAR1 (also known as TGR5 or M-BAR) is the most studied membrane receptor for BAs, which is reported to be $G_{\alpha s}$-coupled (*24*, *25*). To compare BA activation of the GPR39 and GPBAR1 receptors, we tested GPBAR1 activation by all 30 BAs using a cAMP response element (CRE) luciferase assay (fig. S4A) for detecting intracellular cyclic adenosine monophosphate (cAMP) changes (*63*). GPBAR1 was activated by certain BAs (fig. S4, D to H), but not by Zn^{2+} (fig. S4C). Meanwhile, the $G_{\alpha s}$-coupled GPBAR1 could not induce intracellular Ca^{2+} mobilization (fig. S4I). We normalized the E_{max}/EC_{50} value of individual BA for each receptor by the maximum E_{max}/EC_{50} value among 30 BAs, which gave relative intrinsic activity (RAi) values (*64*). As shown in the heatmap of LogRAi (Fig. 2M), the profile of BAs that were able to activate GPR39 was different from that of BAs activating GPBAR1. LCA, DCA, and their T/G conjugates were potent agonists of GPBAR1, while 3-O-sulfation reduced the ability of BAs to activate GPBAR1 (Fig. 2M and fig. S4, D and E) (*65*). Although both GPR39 and GPBAR1 preferred LCA-related BAs, GPBAR1 barely responded to three 3-O-sulfated LCAs which were the most potent agonists of GPR39. Our results suggest that 3-O-sulfation changed the preference of LCA and its T/G conjugates from GPBAR1 to GPR39. In addition, CA7S, a 7-O-sulfated BA that did not activate GPR39 (Fig. 2E), was recently reported to be a potent agonist of GPBAR1 (*66*), but this was not observed by us (fig. S4B).

Mutual potentiation of GPR39 activation between specific BAs and Zn^{2+}

Zn^{2+} potentiated GPR39 activation by most BAs (Fig. 2B); we examined whether BAs could enhance GPR39 activation by Zn^{2+}. We measured GPR39 activation by Zn^{2+} in the presence of individual BAs, and we found that only LCA derivatives, such as LCA, LCAS, and their T/G conjugates, enhanced GPR39 activation by Zn^{2+} (Fig. 3, A to C), with LCAS the most effective (Fig. 3C). Other BAs (Fig. 3C and fig. S5, A to H) did not notably enhanced GPR39 activation by Zn^{2+}.

The concentration of 4 μM Zn^{2+} that we used is much higher than the free Zn^{2+} concentrations in serum (0.09 to 0.42 nM) (*67*) while slightly lower than the total zinc concentration in serum (9 to 18 μM) (*68*). To further quantify the mutual potentiation of GPR39 activation between LCAS and Zn^{2+}, we analyzed the synergistic effects of different concentrations of Zn^{2+} and LCAS. Activation of GPR39 by LCAS was notably shifted by Zn^{2+} at concentrations above 1 μM and vice versa (Fig. 3, D and E). Lower concentrations of ligands could activate GPR39 in the presence of LCAS and Zn^{2+}, and the mutual potentiation between LCAS and Zn^{2+} broadened the dynamic range of GPR39 (Fig. 3F).

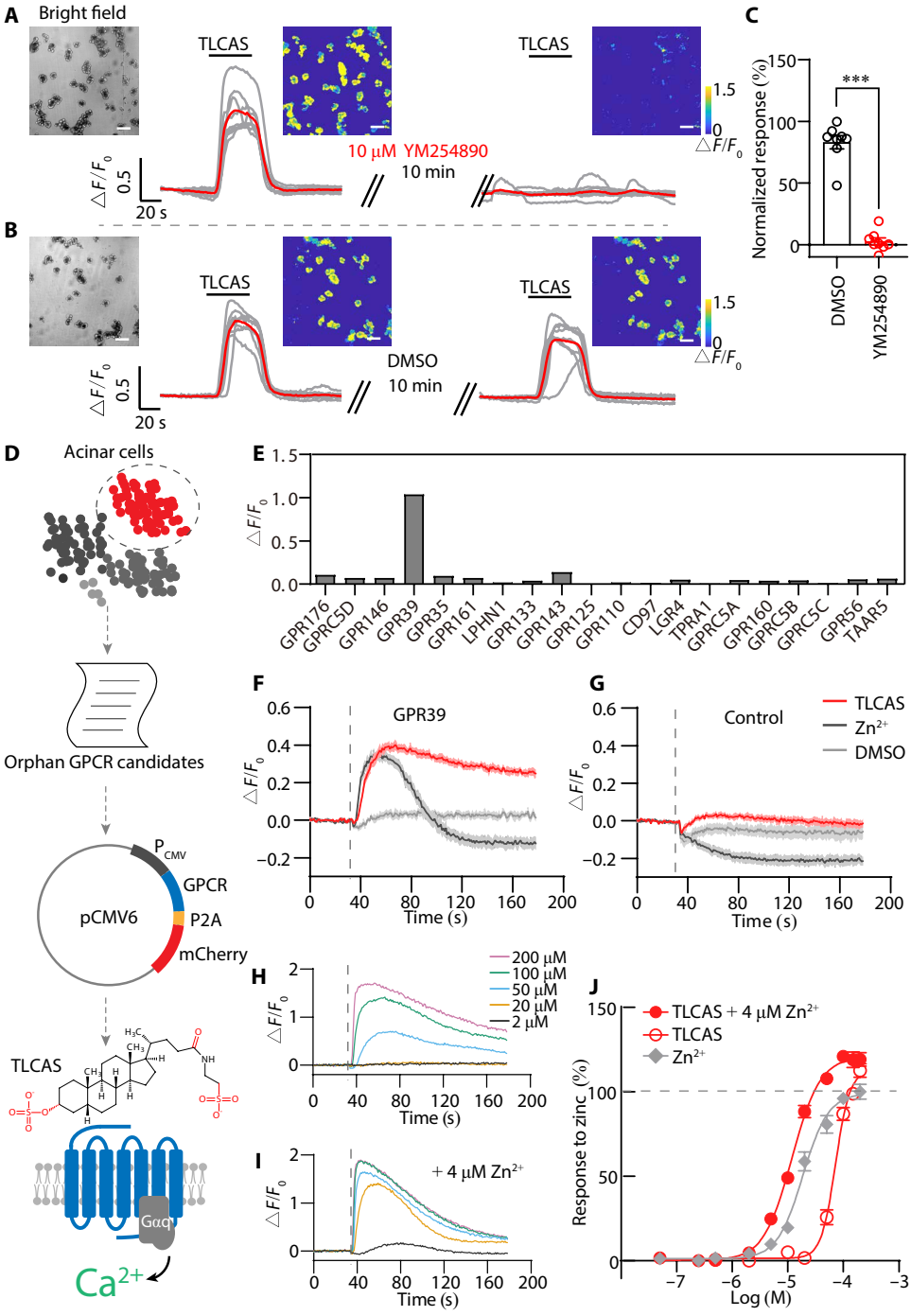

Fig. 1. Search for a TLCAS receptor. (**A** and **B**) Ca^{2+} imaging in isolated pancreatic acinar cells treated with $G_{\alpha q}$-inhibitor YM254890 (A) or vehicle dimethyl sulfoxide (DMSO) (B). Acinar cells were stimulated with two applications of 500 μM TLCAS. Before the second stimulation, the cells were incubated with 10 μM YM254890 (or DMSO) for 10 min. Red traces represent the average responses. Scale bars, 50 μm. (**C**) $G_{\alpha q}$-inhibitor YM254890 totally diminished the Ca^{2+} elevation induced by TLCAS in acinar cells. The values represent the responses of the second stimulation, which normalized to responses of the first stimulation. Two-tailed unpaired Student's *t* test was used (***$P < 0.001$, $n = 8$ in each group). (**D**) A schematic diagram of our GPCR screening strategy. Orphan GPCRs highly expressed in pancreatic acinar cells were cloned and expressed in human embryonic kidney (HEK) 293T cells expressing $G_{\alpha 15}$-GCaMP6s, and possible activation of each receptor by TLCAS was measured by Ca^{2+} imaging. (**E**) Results of the intracellular Ca^{2+} changes mediated by candidate GPCRs in response to 200 μM TLCAS. (**F** and **G**) Real-time FLIPR fluorescence curves of intracellular Ca^{2+} changes induced by 200 μM TLCAS or 200 μM Zn^{2+} in GPR39-expressing cells (F) or the sham-transfected cells (G). The dotted line indicates the time points for the administration of agents or vehicles. (**H**) Concentration-dependent activation of GPR39 by TLCAS. Results from a stable HEK293T cell line expressing the GPR39 are shown here. (**I**) Zn^{2+} enhancement of GPR39 activation by TLCAS. Cells were incubated with 4 μM Zn^{2+} in the recording buffer for 5 min before the FLIPR assay, and the concentrations of TLCAS were similarly color-indicated as those in (H), except that 4 μM Zn^{2+} was included for all concentrations of TLCAS. (**J**) Dose curves of TLCAS and Zn^{2+} in GPR39 activation.

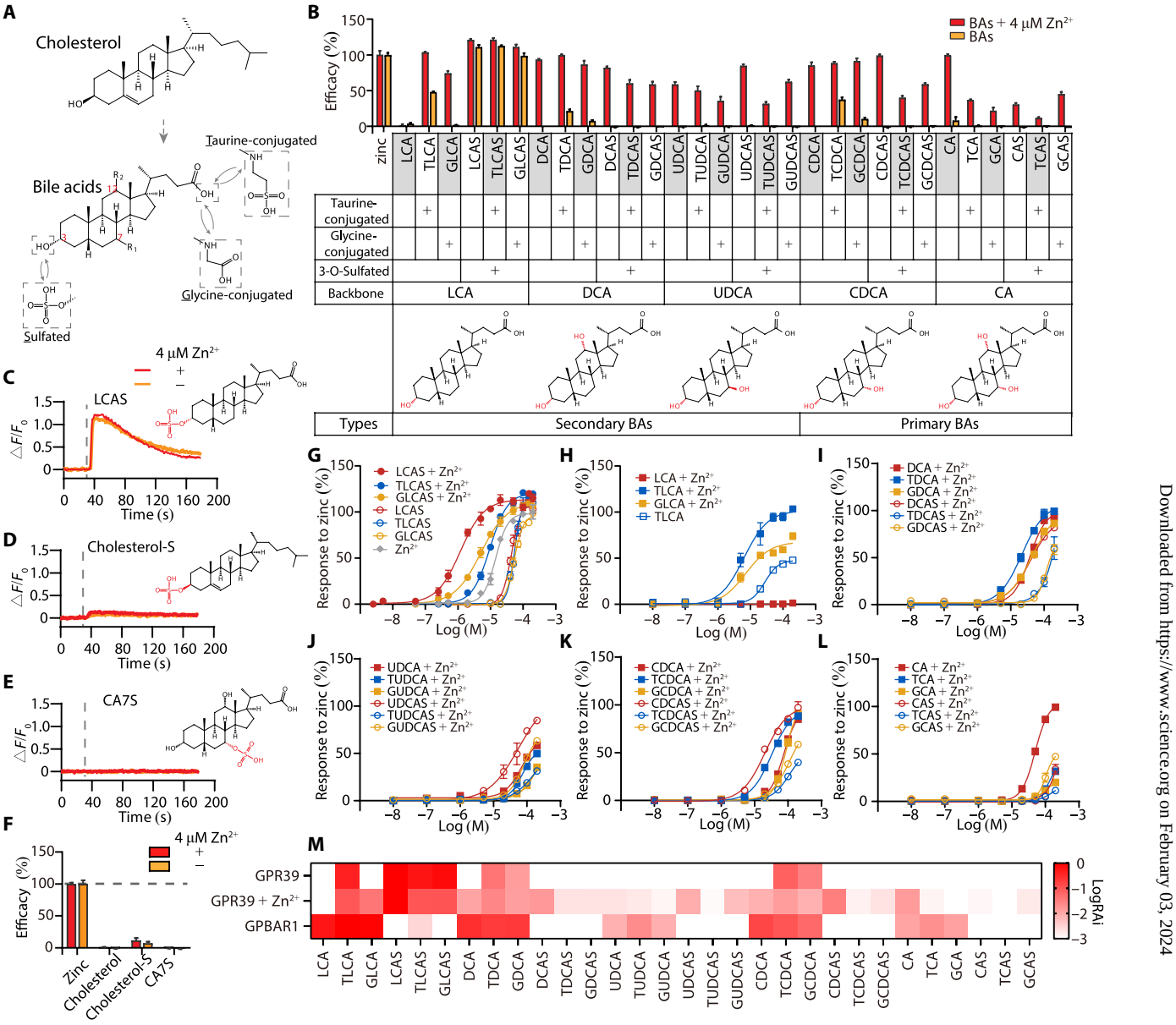

Fig. 2. Characterization of GPR39-mediated activation by BAs. (**A**) Structures of cholesterol and BAs. BAs are synthesized from cholesterol and can be modified by sulfate, and amidated by taurine (or glycine). (**B**) Efficacy of BAs in activating GPR39 in the presence or absence of 4 μM Zn^{2+} (means ± s.e.m.; $n = 3$ or 4 in each group). All values were normalized to that of 200 μM Zn^{2+}. Potency values of 200 μM deoxycholic acid (DCA) and chenodeoxycholic acid (CDCA) in the absence of Zn^{2+} were set to zero. Detailed values are shown in fig. S8. (**C** to **E**) Real-time FLIPR fluorescence curves of intracellular Ca^{2+} changes induced by LCAS, cholesterol-S, and CA7S in GPR39-expressing cells in the presence or absence of 4 μM Zn^{2+}. All compounds are 200 μM and dotted lines indicate the time points for administration of agents. (**F**) Efficacy of cholesterol, LCAS, cholesterol-S, and CA7S in the presence or absence of 4 μM Zn^{2+} (means ± s.e.m.; $n = 4$ in each group). All values were normalized to that of 200 μM Zn^{2+}. (**G** and **H**) Dose-response curves of LCA derivatives in the presence or absence of 4 μM Zn^{2+}. Dose-response curves of DCA derivatives (**I**), UDCA derivatives (**J**), CDCA derivatives (**K**), and CA derivatives (**L**) in the presence of 4 μM Zn^{2+}. Responses were normalized to 200 μM Zn^{2+}. Median effective concentration (EC_{50}) values are shown in fig. S8. (**M**) Heatmap of the LogRAi (logarithm base 10) values for GPR39- and GPBAR1-mediated activation by BAs. Values are shown in fig. S8.

Evolution of GPR39 from a BA receptor to a BA and Zn^{2+} receptor

Amino acid residues histidine (H) at positions 17 (H17) and 19 (H19) of the GPR39 protein have been found previously to be required for its mediation of cellular responses to Zn^{2+} and that H17A/H19A double mutant with histidine changed to alanine (A) could not mediate any Ca^{2+} response to Zn^{2+} (*69*). We tested whether GPR39 required H17 and H19 to respond to BAs by expressing H17A/H19A mutant in HEK293T cells.

While H17A/H19A mutations abolished GPR39 mediation of Zn^{2+}-induced Ca^{2+} elevation, they did not reduce GPR39 mediation of BA-induced Ca^{2+} elevation in the absence of Zn^{2+} (Fig. 4A). Ca^{2+} elevation mediated by the H17A/H19A mutant GPR39 to LCAS, TLCAS, GLCAS (Fig. 4B), and TLCA (Fig. 4C) were not notably

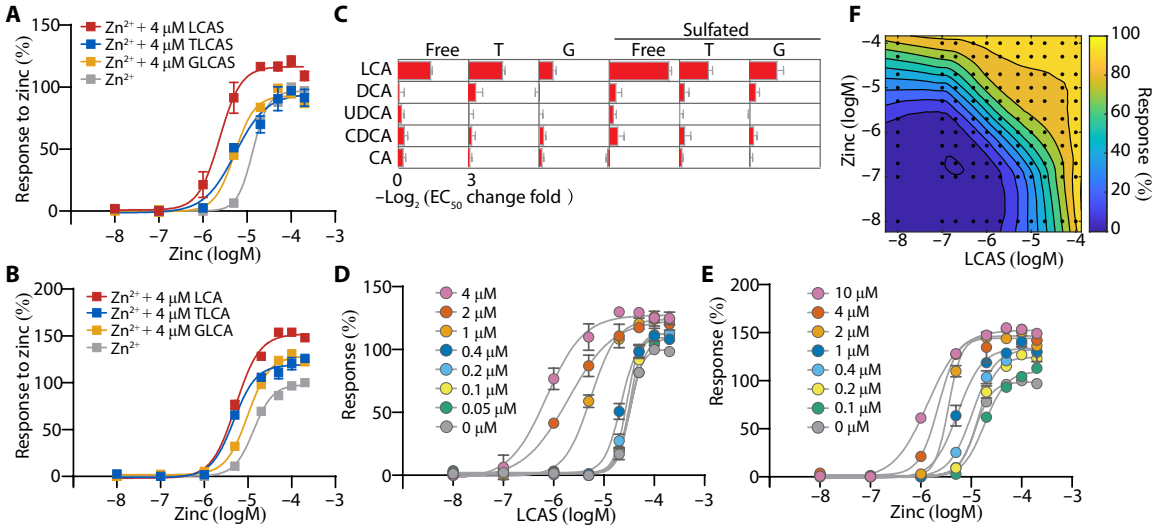

Fig. 3. LCA derivatives potentiate GPR39 activation by Zn^{2+}. (**A** and **B**) The allosteric effect of LCA derivatives on GPR39 activation by Zn^{2+}. Responses were normalized to 200 μM Zn^{2+}. (**C**) The potentiation of 30 BAs on GPR39 activation by Zn^{2+}. The ratio of EC_{50} of Zn^{2+} in the presence of BAs to EC_{50} of Zn^{2+} in the absence of BAs was calculated, and the value was logarithmically (with a base of 2) transformed (means ± s.e.m.; $n = 3$ or 4 in each group). Values are shown in fig. S8. (**D**) The dose curves of GPR39 activated by LCAS in the presence of indicated concentrations of Zn^{2+}. Responses were normalized to 200 μM LCAS. (**E**) The dose curves of GPR39 activated by Zn^{2+} in the presence of indicated concentrations of LCAS. Responses were normalized to 200 μM Zn^{2+}. (**F**) The *LOWESS*-fit response surface of GPR39 costimulated with combinations of LCAS and Zn^{2+}. Responses were normalized to the maximum response among all experimentally tested points (black dots).

different from that mediated by the wild-type (WT) GPR39 (Fig. 2, G and H). Moreover, responses mediated by the H17A/H19A mutant to DCA and CDCA derivatives (Fig. 4A) were larger than those mediated by the WT GPR39 (Fig. 2B).

Zn^{2+} potentiation of cellular responses to BAs was reduced in the H17A/H19A mutant. In H17A/H19A-transfected cells, CA derivatives and UDCA derivatives barely triggered Ca^{2+} elevation even in the presence of Zn^{2+} (Fig. 4A). As shown in Fig. 4 (B and C), only the dose-response curves of LCAS and TLCA among eight BAs showed a notable left shift in the presence of Zn^{2+}. These results indicated that H17 and H19 were required for GPR39 mediation of cellular responses to Zn^{2+} alone and Zn^{2+} potentiation of GPR39 responses to BAs (except LCAS and TLCA), but not required for GPR39 mediation of signaling by BAs alone or Zn^{2+} potentiation of GPR39 responses to LCAS or TLCA.

Analysis of GPR39 protein sequences in different species indicated that H17 and H19 were not conserved in all species (Fig. 4D): They were not present in fish, but emerged in amphibians, and present in reptiles, birds, and mammals. We cloned GPR39 receptors from different species and expressed them in HEK293T cells. The GPR39 from the chicken (*Gallus Gallus*), the gecko (*Gekko japonicus*), and the frog (*Xenopus laevis*) showed strong dose-dependent responses to both LCAS and Zn^{2+} (Fig. 4, E to G). The zebrafish (*Danio rerio*) GPR39 (zfGPR39 for short) could be activated by BAs robustly, while it mediated little response to Zn^{2+} (Fig. 4H). Similar to the H17A/H19A mutant, zfGPR39 mediated responses to DCA and CDCA derivatives in the absence of Zn^{2+} (Fig. 4H), which showed a much broader BAs preference than mouse and human GPR39 (Fig. 2B and fig. S3A). On the other hand, different from the H17A/H19A mutant, BA activation of zfGPR39 could be enhanced by Zn^{2+} as the dose curves of all eight BAs were shifted to the left (Fig. 4, I and J).

To test the activation of GPR39 by the physiological BAs, we extracted total BAs from pig and carp raw bile using solid-phase extraction (SPE) (Fig. 4K). Diluted bile extracts were applied to GPR39-expressing HEK293T cells. Despite the presence of background fluorescence in mock-transfected cells, 1/400 diluted pig (Fig. 4L) and carp (Fig. 4M) bile extracts were observed to notably increase the cytosolic Ca^{2+} in cells expressing mouse GPR39, its H17A/H19A mutant, and zfGPR39 (Fig. 4, L to N). GPR39 activation by bile extracts was also dose-dependent and potentiated by Zn^{2+} (fig. S6, A to J).

Apart from C24 BAs, C27 bile alcohols are commonly found in fish bile (*70*). We examined the activity of 5b-cholestanpentol, a C27 bile alcohol, on zfGPR39. 5b-cholestanpentol had minimal effects on zfGPR39 activation, even in the presence of 4 μM Zn^{2+} (fig. S6, N and O). By contrast, 5b-cholestanpentol robustly activated mouse GPR39, regardless of the presence or absence of Zn^{2+} (fig. S6, L, M, and P).

Thus, the evolutionarily earlier GPR39 does not mediate responses to Zn^{2+} alone. Zn^{2+} could modulate BAs stimulation of zfGPR39. Later in evolution, GPR39 mediates responses to fewer types of BAs but gains responses to Zn^{2+} alone. In other words, GPR39 was primarily a BA receptor to begin with but can also serve as a Zn^{2+} receptor later.

GHSR activation by BAs

GPR39 belongs to the ghrelin receptor subfamily (*50*) that contains receptors for ghrelin, motilin, neuromedin U, and neurotensin (Fig. 5A). Although GPR39 shows structural similarities to these homologs, four endogenous peptides did not activate GPR39 (Fig. 5, B and C).

We tested whether receptors in the phylogenetic tree close to GPR39 could be activated by BAs. We expressed them in HEK293T cells to detect intracellular Ca^{2+} signaling changes. GHSR, the ghrelin receptor (*71*), was activated by BAs including LCA, TLCA, GLCA, DCA, TDCA, GDCA, UDCA, and CDCA (Fig. 5, D and E).

By pretreating with the GHSR-specific antagonist JMV-2959 (*72*), the Ca^{2+} responses induced by ghrelin (Fig. 5F), UDCA (Fig. 5G),

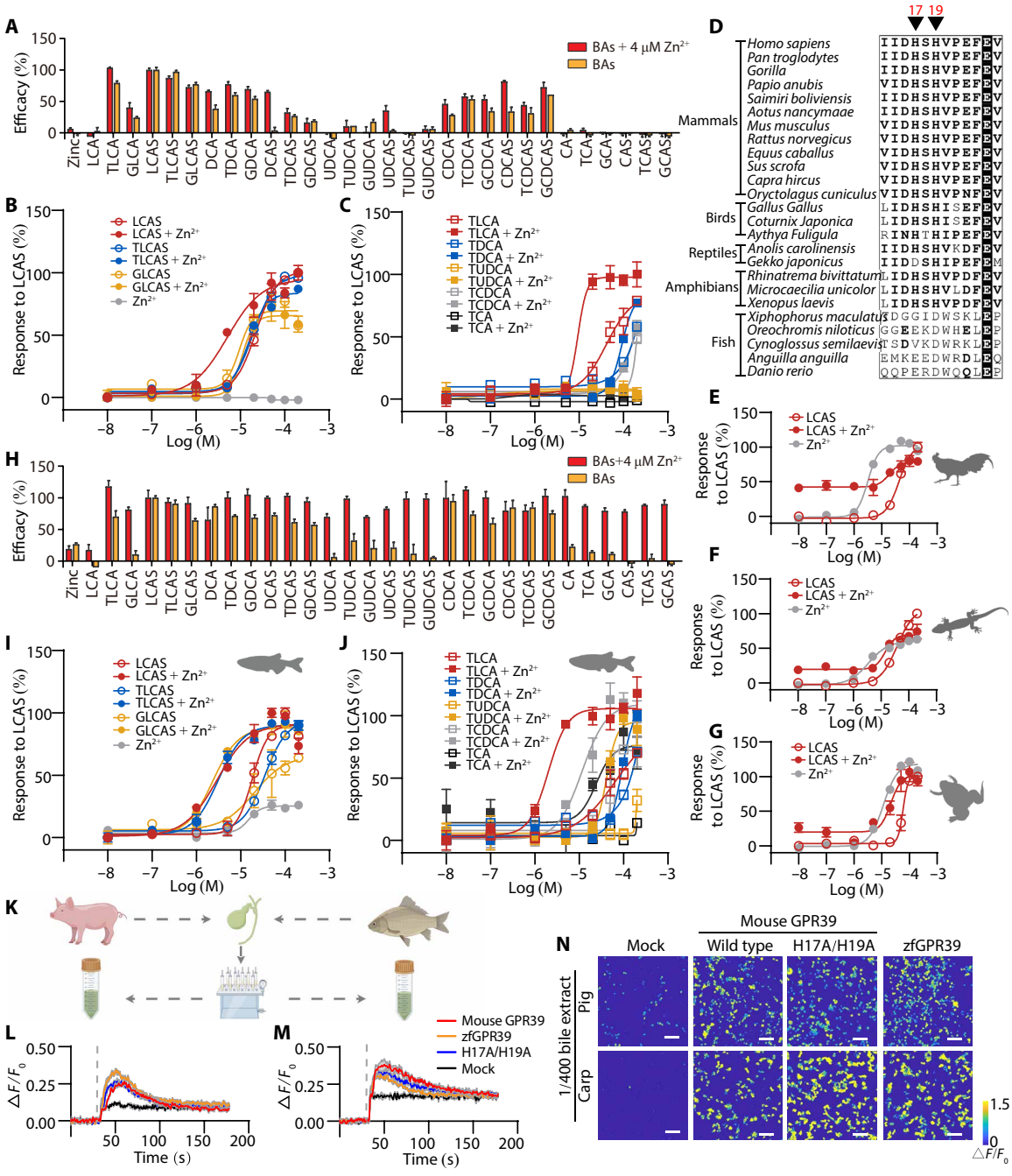

Fig. 4. Evolution of Zn^{2+} responsiveness after BA responsiveness in GPR39. (**A**) Efficacy of BAs in Zn^{2+} insensitive GPR39 mutant H17A/H19A activation in the presence or absence of 4 μM Zn^{2+} (means ± s.e.m.; $n = 3$ or 4 in each group). All values were normalized to the efficacy of 200 μM LCAS. (**B** and **C**) Dose-response curves of H17A/H19A mutant form of GPR39 by BAs. Responses were normalized to 200 μM LCAS. (**D**) Multiple sequence alignment of GPR39 receptors from different species. The ClustalW program was used for sequence alignment, and the figure was generated by ESRipt3. For each sequence, the accession number is shown in table S1. (**E** to **G**) Activation of *G. Gallus* GPR39 (E), *G. japonicus* GPR39 (F), and *X. laevis* GPR39 (G) by LCAS and Zn^{2+}. (**H**) Efficacy of BA activation of the zfGPR39 in the presence or absence of 4 μM Zn^{2+} (means ± s.e.m.; $n = 3$ or 4 in each group). All values were normalized to the efficacy of 200 μM LCAS. (**I** and **J**) Dose-response curves of the zfGPR39 by BAs. Responses were normalized to 200 μM LCAS. (**K**) Raw bile samples from pigs and carp were subjected to extraction using a C18 solid-phase cartridge. The crude extracts were employed to assess the responses of GPR39 to both pig and fish bile. (**L** and **M**) FLIPR fluorescence curves of intracellular Ca^{2+} changes induced by 1/400 diluted pig (L) and carp (M) bile extracts in HEK293T cells expressing mouse GPR39, zfGPR39, H17A/H19A mutant or mock-transfected cells. Dotted lines indicate the time points for the administration of agents. (**N**) Ca^{2+} imaging of GPR39-expressing HEK293T cells responding to 1/400 diluted pig and carp bile extracts. Scale bars, 100 μm.

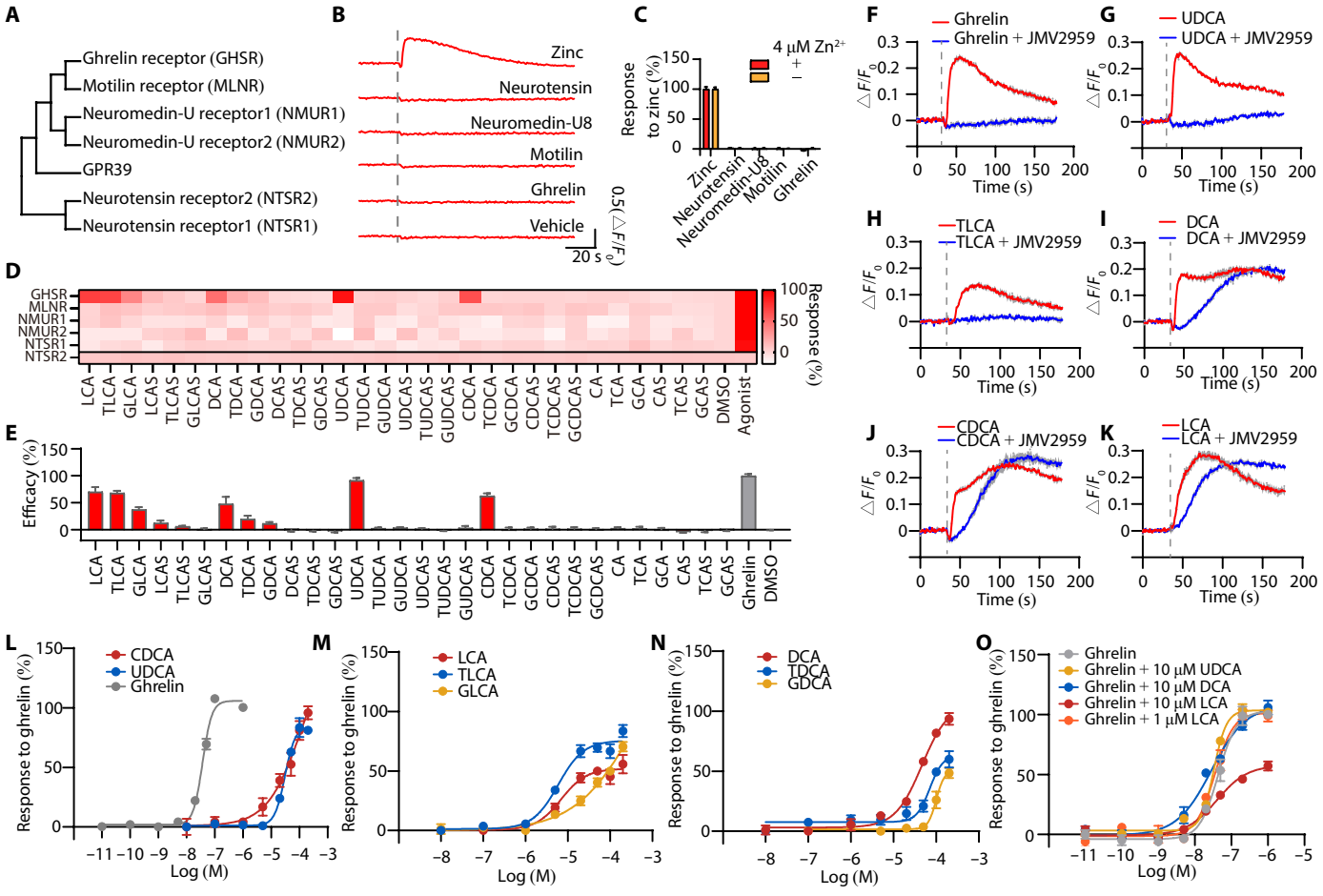

Fig. 5. GHSR is activated by BAs. (**A**) The phylogenetic tree of the ghrelin receptor subfamily. The tree was constructed by MEGA11 and the accession number of each sequence is shown in table S1. (**B** and **C**) Testing the activation of GPR39 by peptides using FLIPR. (B) Typical real-time FLIPR fluorescence curves in the presence of 4 μM Zn^{2+} and (C) efficacy normalized to 200 μM Zn^{2+} (means ± s.e.m.; $n = 4$ in each group). Each used peptide was 1 μM. (**D**) Activation of GPR39-related receptors by BAs was tested using FLIPR. Receptors were expressed in HEK293T cells expressing $G_{\alpha 15}$-GCaMP6s, and the activation of each receptor by 200 μM BAs was measured. One micromolar of ghrelin (for GHSR), 200 μM roxithromycin (for MLNR), 1 μM neuromedin-U8 (for NMUR1/2), and 1 μM neurotensin (for NTSR1/2) were used as positive agonists. Responses were normalized to the corresponding agonists. DMSO (1%) was used as a negative control. NTSR2 could not be activated by BAs or neurotensin, and the responses of NTSR2 were expressed as $\triangle F/F_0$. (**E**) Efficacy of BAs in activating GHSR (means ± s.e.m.; $n = 6$ in each group). All values were normalized to that of 1 μM ghrelin. All BAs were 200 μM. (**F** to **K**) Real-time FLIPR fluorescence curves of intracellular Ca^{2+} changes induced by ghrelin (F), UDCA (G), TLCA (H), DCA (I), CDCA (J), and LCA (K) in GHSR-expressing cells in the presence or absence of 10 μM GHSR antagonist JMV2959. Ghrelin (F) was 100 nM and all BAs were 200 μM. Dotted lines indicate the time points for the administration of agents. (**L** to **N**) The dose curves of GHSR activated by BAs. Responses were normalized to that of 1 μM ghrelin. (**O**) The dose curves of GHSR activated by ghrelin in the presence of indicated BAs. Responses were normalized to that of 1 μM ghrelin.

and TLCA (Fig. 5H) were totally abolished. In GHSR-expressing HEK293T cells, Ca^{2+} elevations induced by 200 μM DCA and CDCA were characterized by a rapid rise (Fig. 5, I and J). In the presence of the GHSR blocker JMV-2959, Ca^{2+} elevations were characterized by a slow rise (Fig. 5, I and J), which were similar to nonspecific Ca^{2+} elevations induced by 200 μM DCA and CDCA in mock-transfected cells (fig. S2, A and B). Ca^{2+} mobilization induced by LCA in GHSR-expressing cells could be moderately but not fully inhibited by JMV-2959 (Fig. 5K). All eight BAs activated GHSR in a dose-dependent manner (Fig. 5, L to N), and the maximal efficacy of UDCA, DCA, and CDCA was comparable to ghrelin, while TLCA and LCA showed a relatively higher sensitivity but a lower efficacy compared with UDCA, DCA, and CDCA.

We examined whether BAs could potentiate GHSR activation by its endogenous peptide ligand ghrelin. Ten micromolar of UDCA and DCA did not potentiate or attenuate the action of ghrelin (Fig. 5O). Pretreating GHSR-expressing cells with 10 μM LCA attenuated the effect of ghrelin (Fig. 5O). This may result from the activation and desensitization of GHSR by 10 μM LCA, and there was no effect on the activation of GHSR using 1 μM LCA (Fig. 5O).

Requirement of GPR39 in pancreatic acinar cells for Ca^{2+} elevation induced by BAs

Results shown above indicate that the exogenous GPR39 introduced to HEK293T cells could mediate Ca^{2+} elevation in response to BAs. While these results support that GPR39 is sufficient for BA activation, they do not answer the question of whether GPR39 is necessary in normal cells for mediating cellular responses to BAs.

Gpr39 expression has been found in the pancreas (*51*, *52*, *73*). We have generated hemagglutinin (HA)-tagged GPR39 mice ($Gpr39^{HA}$)

(Fig. 6A). Immunostaining of *Gpr39*^{HA} pancreatic cryosections stained with anti-HA antibody revealed that GPR39 was localized on the plasma membrane of acinar cells (Fig. 6B). To investigate the role of GPR39 in pancreatic acinar cells, we have generated *Gpr39* knockout mice (*Gpr39*^{KO}) (Fig. 6A). After backcrossing, we obtained mice with the WT (*Gpr39*$^{+/+}$), heterozygous (*Gpr39*$^{+/-}$), or homozygous mutant genotypes (*Gpr39*$^{-/-}$). In freshly isolated acinar cells from *Gpr39*$^{+/+}$ mice, intracellular Ca^{2+} elevation was observed after the application of either LCAS (Fig. 6, C and E, top) or TLCAS (fig. S7, A and C, top). Acinar cells from GPR39$^{+/-}$ mice showed attenuated responses to LCAS (Fig. 6, C and E, middle) and TLCAS (fig. S7, A and C, middle). In acinar cells from *Gpr39*$^{-/-}$ mice, little response to LCAS (Fig. 6, C and E, bottom) or TLCAS (fig. S7, A and C, bottom) was observed.

Although a previous report suggested that GPBAR1 was responsible for the Ca^{2+} signaling in acinar cells induced by TLCAS (*37*),

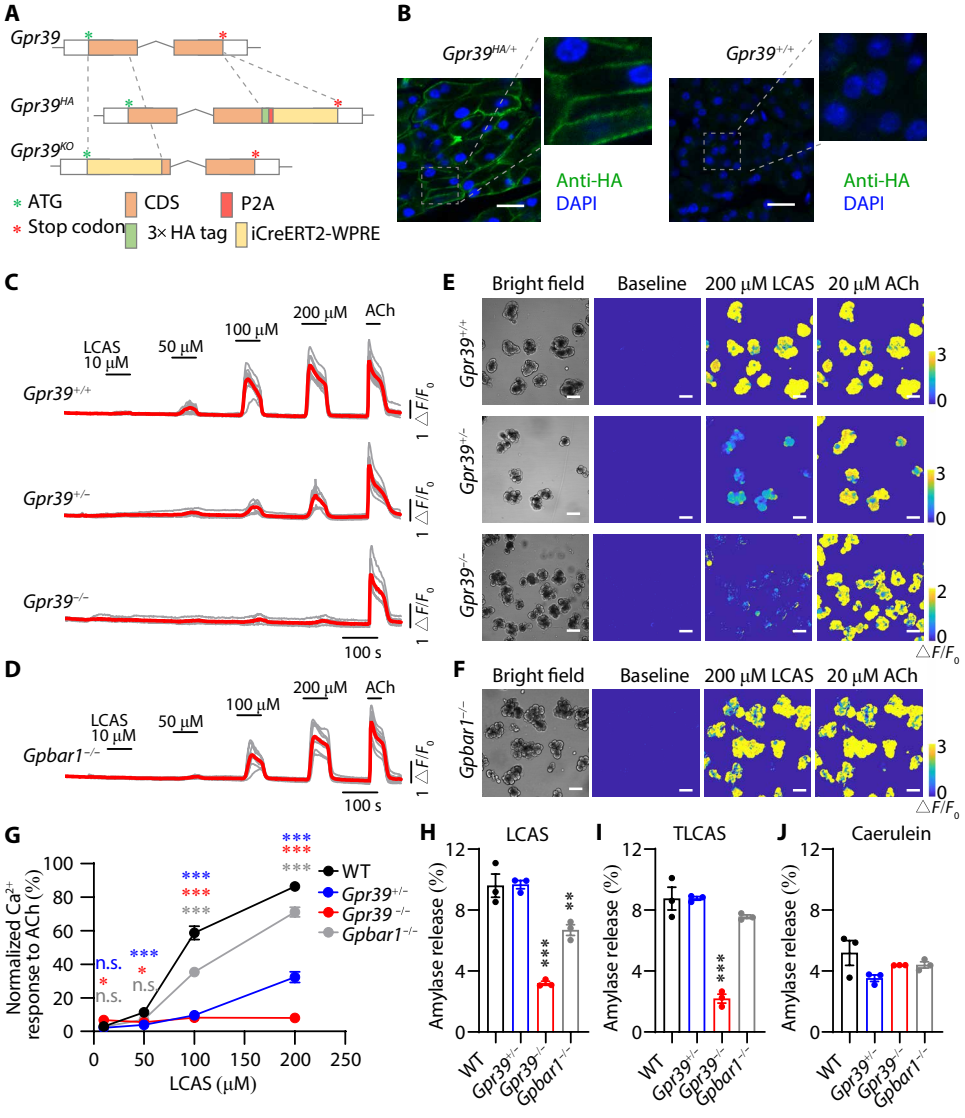

Fig. 6. Requirement of GPR39 in pancreatic acinar cells for BA responses. (**A**) A schematic diagram of the generation of *Gpr39*^{HA} and *Gpr39*^{KO} mice. Briefly, *Gpr39*^{HA} mice were generated by the insertion of three repeats of the HA epitope (3× HA) followed by P2A-iCreERT2-WPRE at the C terminus of GPR39. *Gpr39*^{KO} mice were generated by replacing parts of exon 1 of the *Gpr39* gene with iCreERT2-WPRE. (**B**) Immunofluorescence staining of *Gpr39*^{HA} mice pancreatic sections with anti-HA antibody showed that GPR39 expressed in acinar cells. Scale bars, 20 μm. (**C** and **D**) Intracellular Ca^{2+} elevation induced by LCAS in acinar cells. Increasing concentrations of LCAS were used (from 10 to 200 μM). ACh (20 μM) was used as a positive control at the end of each experiment to ensure the responsiveness of the acinar cells. Red traces represent the average responses. (**E** and **F**) Representative pseudo-colored images of intracellular Ca^{2+} elevation in acinar cells before and after application of 200 μM LCAS. Scale bars, 50 μm. (**G**) Ca^{2+} signal peaks of indicated genotypes stimulated by LCAS of different concentrations, normalized to that of 20 μM ACh. Each genotype was compared with the WT with the same concentration of LCAS. One-way analysis of variance (ANOVA) with Tukey's multiple comparisons posttest was used (***$P < 0.001$, **$P < 0.01$, *$P < 0.05$, and n.s. $P > 0.05$; means ± s.e.m). Colored stars were used to distinguish different genotypes. (**H** to **J**) BA-induced discharges of amylase were reduced in acini from GPR39 knockout mice. The net amylase release of acini treated with 500 μM LCAS (H), 500 μM TLCAS (I), or 1 nM caerulein (J) was shown as a percentage of total amylase. One-way ANOVA with Tukey's multiple comparisons posttest was made to the WT group (***$P < 0.001$ and **$P < 0.01$; means ± s.e.m).

we observed robust Ca^{2+} increases induced by 200 μM LCAS (Fig. 6, D and F) and TLCAS (fig. S7, B and D) in acinar cells isolated from GPBAR1 knockout (*Gpbar1*$^{-/-}$) mice, which were comparable to that of WT mice. For further comparison, we normalized the peak Ca^{2+} values with that induced by acetylcholine (ACh). Results show that the Ca^{2+} elevation induced by LCAS (Fig. 6G) or TLCAS (fig. S7E) at all tested concentrations (50, 100, 150, and 200 μM) was basically absent when the *Gpr39* gene was deleted. Although Ca^{2+} signaling was decreased in *Gpbar1*$^{-/-}$ mice, Ca^{2+} signaling in *Gpbar1*$^{-/-}$ mice was still larger than those in *Gpr39*$^{+/-}$ mice (Fig. 6G and fig. S7E). Furthermore, Ca^{2+} elevation in acinar cells was not observed upon exposure to BAs that have the ability to increase cAMP via GPBAR1 or the GPBAR1 agonist INT-777, as shown in fig. S7 (F to H). These results support that GPR39 plays an essential role in mediating Ca^{2+} elevation in response to BAs, whereas the role of GPBAR1 in this regard is less important.

The secretion of acinar cells is dependent on intracellular Ca^{2+} (*74*), and the TLCAS-stimulated amylase discharge was reported to be Ca^{2+}-dependent but GPBAR1-independent (*37*). We measured the net amylase discharge of acinar cells stimulated by LCAS, TLCAS, and another secretagogue caerulein. Deleting *Gpr39* significantly reduced the amylase release of acinar cells induced by LCAS (Fig. 6H) and TLCAS (Fig. 6I) but not caerulein (Fig. 6J). Deletion of *Gpbar1* did not alter the amylase discharge induced by TLCAS and caerulein (Fig. 6, I and J). Amylase release induced by LCAS was reduced in pancreatic acinar cells from *Gpbar1*$^{-/-}$ mice but still higher than that of pancreatic acinar cells from *Gpr39*$^{-/-}$ mice (Fig. 6H). Again, the role of GPR39 is more important than GPBAR1. These results indicate that GPR39 is necessary for BA stimulation of Ca^{2+} elevation in, and amylase release from, pancreatic acinar cells.

Role of GPR39 in BA-induced AP

Intracellular Ca^{2+} overload and necrosis of acinar cells were thought to be the early events of AP (*12*, *14*, *17*, *75*). We used *Gpr39* knockout mice to test GPR39's involvement in BA-induced AP.

First, we tested acinar cells isolated from mice. Cell injuries were assessed by propidium iodide (PI) uptake and the release of lactate dehydrogenase (LDH). LCAS, TLCAS, or caerulein increased PI uptake into isolated acinar cells of WT mice (Fig. 7A). LCAS, TLCAS, or caerulein increased LDH release from isolated acinar cells of WT mice (Fig. 7B). Knockout of *Gpr39*, but not that of *Gpbar1*, decreased PI uptake and LDH leakage induced by LCAS or TLCAS, but did not affect those induced by caerulein (Fig. 7, A and B). Cell injuries induced by high concentrations of TLCAS and caerulein were accompanied by cell blebbing (*76*, *77*). These morphological changes were observed in acinar cells isolated from WT and *Gpbar1*$^{-/-}$ mice after the stimulation of LCAS and TLCAS, but not in acinar cells isolated from *Gpr39*$^{-/-}$ mice under the same conditions (Fig. 7C).

Next, we used an in vivo AP model with an infusion of BAs into the pancreatic duct (Fig. 7D) (*78*, *79*). Serum levels of amylase and lipase were significantly increased by LCAS in WT (*Gpr39*$^{+/+}$) mice, but not in *Gpr39*$^{-/-}$ mice (Fig. 7E). Histological examinations showed increased edema, inflammation, and necrosis induced by LCAS in WT mice (Fig. 7, F and G). LCAS-induced inflammation and necrosis were both reduced in *Gpr39*$^{-/-}$ mice (Fig. 7G). Although TLCAS-induced pancreatitis was weaker than that of LCAS (fig. S7I), *Gpr39*$^{-/-}$ mice still exhibited lower histopathology scores in TLCAS-induced AP models (fig. S7, J and K). These results indicated that GPR39 was involved in the pathogenesis of biliary AP in vivo.

DISCUSSION

A cDNA encoding the GPR39 receptor was cloned in 1997 (*80*). It was found in 2004 that GPR39 could be activated by Zn^{2+} (*56*). The report of obestatin as the endogenous ligand of GPR39 (*81*) could not be reproduced, so Zn^{2+} was the only known endogenous ligand of GPR39 for a long time (*55*, *57*, *82*, *83*). Here, we have shown that GPR39 is a membrane receptor for BAs. Zn^{2+} has been demonstrated to function as an allosteric modulator of various GPCRs (*84*). For GPR39, the binding sites of Zn^{2+} are located in the N-terminal extension (H17 and H19), which is distinct from the common orthosteric binding pockets in the upper region of the transmembrane domain and extracellular loop 2 (*69*, *85*). The finding that the activation of GPR39 by BAs was independent of Zn^{2+} binding sites suggests Zn^{2+} acts as an allosteric ligand of GPR39 and BAs serve as the endogenous orthosteric ligands.

BA signaling through GPR39 may have other functional roles in physiological and pathological conditions. For example, GPR39 is highly expressed in the liver and the intestine (*51*, *52*). BAs are present in hepatobiliary and intestinal tracts, ranging from 1 to 200 mM (*86*). Diluted bile extracts activated the GPR39 (Fig. 4, L to N). The overlapping of the GPR39 expression pattern and BA distribution supports the possibility that GPR39 senses BA signaling in the intestines. GPR39 is abundantly expressed in the epithelial cells of the digestive system which are the key innate immune barrier against microbes in the gut (*51*, *52*). GPR39 activation regulates pH homeostasis in colonocytes and enhances epithelial tight junction, which is crucial for the integrity of the intestinal mucosal barrier (*53*, *87*). BA signaling sensed by the GPR39 receptor may potentially enhance the tight junctions of epithelial cells.

The functional significance of BA and Zn^{2+} potentiation will also be an interesting avenue for future studies. In the intestinal epithelium, Zn^{2+} is co-released with antimicrobial components from Paneth cells through vesicles in response to pathogens (*88*). In this context, does Zn^{2+} signaling from Paneth cells interact with BAs signaling to regulate the integrity of epithelial cells? Here, we have found the pathological roles of GPR39 activation by high concentrations of BAs in the context of biliary AP. However, under physiological conditions, the concentration of BAs that the pancreas is exposed to is much lower (0.2 to 22 μM in the systemic plasma) (*86*). It is worth noting that Zn^{2+} is co-released with insulin from pancreatic β cells and that GPR39 is also expressed in islets (*52*, *89*). It will be curious to know whether GPR39 is a Zn^{2+} sensor in the pancreas and whether blood-circulating BAs, especially 3-O-sulfated lithocholic acids, play a role in regulating pancreatic islets and exocrine acinar cells function during insulin secretion. More broadly, the roles of BAs and Zn^{2+} in other contexts remain to be investigated.

Sulfation was thought to be a pathway for BA detoxification (*90*) with the 3-O-sulfation as the major form in humans (*91*–*93*). Sulfated BAs have been considered the final metabolites of BAs (*90*), as they are easily excreted from the body. Modification by sulfation can improve the electronegativity of BAs and greatly increase their solubility in water. The detergent properties of sulfated BAs are weaker than non-sulfated BAs, while the critical micellar concentration of sulfated BAs becomes higher (*94*). The proportion of sulfated BAs

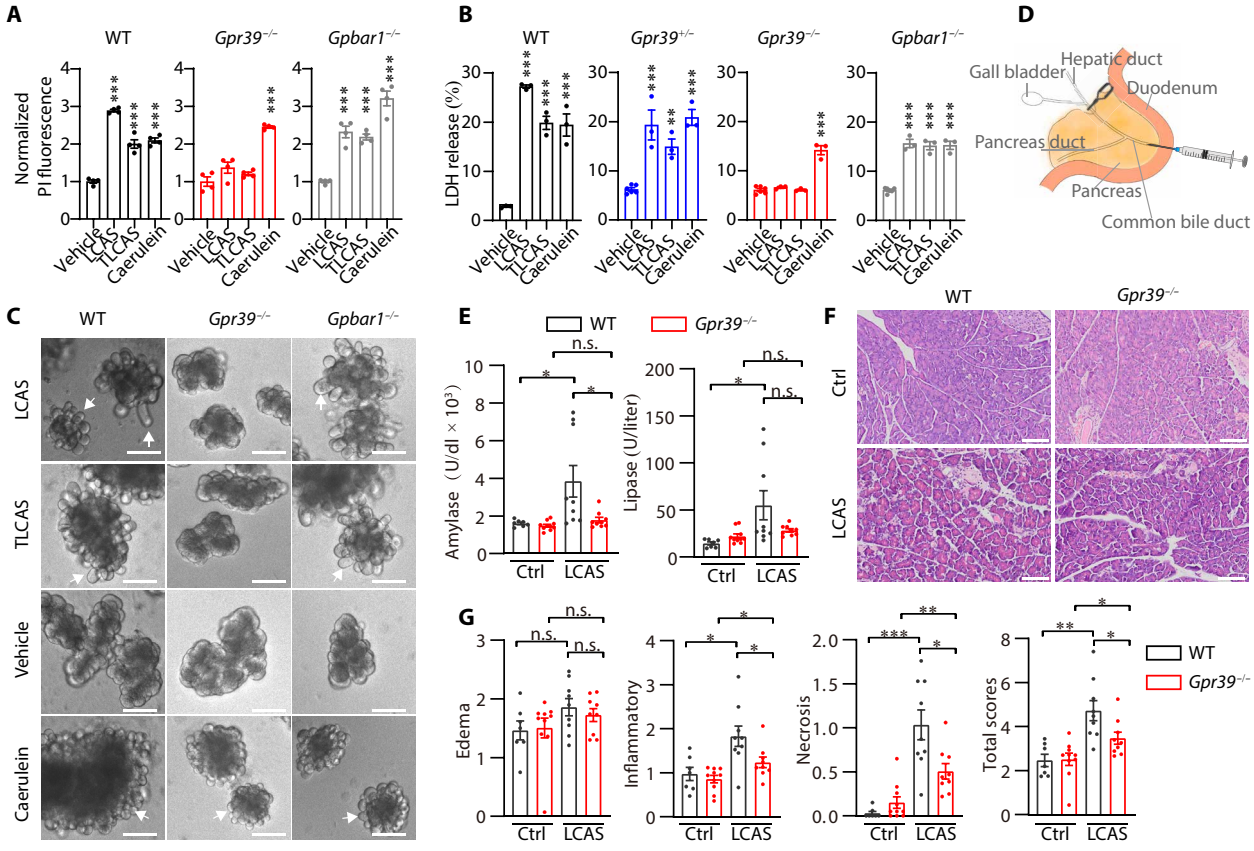

Fig. 7. Deleting GPR39 ameliorates pancreatic injuries by BA-induced AP. (**A** and **B**) PI uptake (A) and LDH leakage (B) induced by LCAS and TLCAS required GPR39 but not GPBAR1. Acinar cells were incubated with LCAS (500 μM), TLCAS (500 μM), or caerulein (100 nM) for 4 hours. PI fluorescence was normalized to that of vehicle-treated control and the net LDH leakage was expressed as a percentage of the total LDH. One-way ANOVA with Tukey's multiple comparisons posttest was made to the vehicle group (**$P < 0.01$ and ***$P < 0.001$; means ± s.e.m). (**C**) Representative images of acinar cell blebbing. Blebbing is denoted by arrows. Scale bars, 100 μm. (**D**) A schematic diagram of the pancreatic duct infusion-induced AP model. BAs were retrogradely injected into the pancreas through the pancreatic duct to induce AP. (**E**) Amylase and lipase levels in the serum of mice after LCAS-induced AP. Two-tailed unpaired Student's *t* test was used (***$P < 0.001$, **$P < 0.01$, *$P < 0.05$, n.s. $P > 0.05$; means ± s.e.m). (**F**) Representative hematoxylin and eosin staining of pancreatic histology in LCAS-induced AP. Scale bars, 50 μm. (**G**) Histopathology scores for edema, inflammatory cell infiltration, acinar cell necrosis, and total scores. Two-tailed unpaired Student's *t* test was used (***$P < 0.001$, **$P < 0.01$, *$P < 0.05$, n.s. $P > 0.05$; means ± s.e.m).

varies between different species. In general, the proportion of sulfated BAs is higher in humans and other primates, but lower in rodents. Sulfated BAs can reach 20% of the total BAs in the human liver, ~30% in the plasma, and ~80% in urine. In mice, the proportion of sulfated BAs is 0.7% in bile, 0.2% in plasma, and 70 to 80% in urine (*93*, *95*). The ratio of sulfation is negatively correlated with the number of hydroxyl groups in BAs. The sulfation ratio of LCA is the highest, followed by DCA, CDCA, and UDCA, with CA being the least sulfated. In human plasma, sulfated CA is only 5% of total CA, sulfated DCA/CDCA/UDCA is between 30 and 60%, but sulfated LCA is 93% of total LCA (*91*, *92*).

The findings of our study indicate that 3-O-sulfated lithocholic acids exhibit a greater propensity to stimulate GPR39, a $G_{\alpha q}$-coupled GPCR, as opposed to GPBAR1, which is $G_{\alpha s}$-coupled. GPBAR1 is a previously known receptor for BAs (*24*, *25*). GPBAR1 plays important roles in enterohepatic recycling of BAs, intestinal motility, energy homeostasis, and inflammation (*28*–*30*, *96*, *97*). The present discovery elucidates a signaling pathway involving 3-O-sulfated lithocholic acids, GPR39, and $G_{\alpha q}$, which is distinct from the previously characterized BAs-GPBAR1-$G_{\alpha s}$ signaling pathway.

If GPR39 is the key in biliary AP pathogenesis, which of the BAs are important for AP? That Zn^{2+} potentiates almost all BAs to activate GPR39 complicates the prediction as to which BA, or all BAs at sufficiently high concentrations, could be involved in AP pathogenesis. It will be interesting to test whether one of the 3-O-sulfated lithocholic acids is more important than other BAs in AP, or that all BAs can contribute to AP. In the latter case, the importance of Zn^{2+} would be increased. Our discovery of GPR39 mediation of BA signaling and its role in AP will stimulate further research into BA functions dependent on GPR39 as well as GPR39 functions related to BAs, suggesting potential therapeutic value for screening of GPR39 antagonists. Because knocking out the GPR39 receptor enhances acinar cell resistance to BAs in vitro and in vivo, GPR39 antagonists may alleviate biliary AP.

MATERIALS AND METHODS

Chemicals and reagents

Details on BAs and pharmacological reagents used in this study are provided in table S2. Pig and carp raw bile were extracted by SPE

(*98*, *99*). Briefly, 0.5 ml of fresh bile was added into 10 ml of hot 95:5 (v/v) mixture of ethanol and methanol. After vortex-mixing and cooling, the sample was centrifuged at 13,000*g* at 4°C for 5 min. The supernatant was diluted with ultrapure water to attain an alcoholic concentration of 10% and the solution was subjected to a C18 solid-phase cartridge (Supelclean LC-18 SPE Tube, bed wt. 2 g, Merck). The cartridge was activated with 10 ml of 100% methanol followed by conditioned with 10 ml of 10% methanol. The processed bile sample (corresponding to 0.5 ml of bile) was passed through the preconditioned cartridge and the cartridge was washed with 10 ml of 10% methanol. The cartridge was lastly eluted with 20 ml of methanol. The eluate was concentrated to dryness with a centrifugal evaporator at 30°C, and dissolved in 0.5 ml of water. This extract served as a substitute for the raw bile.

Analysis of orphan GPCR expression in pancreatic acinar cells

Single-cell RNA-seq dataset of the pancreas was downloaded from ArrayExpress (E-MTAB-5061) (*59*). This dataset includes 3514 single-cell transcriptomes, and we extracted 112 of them from healthy human pancreatic acinar cells. The mean expression level of each GPCR among these acinar cells was calculated. The list of orphan GPCRs referred to the IUPHAR database (*46*).

Molecular biology

All 20 candidate GPCRs and 6 GPR39-related receptors are of human origin and were purchased from GenScript (Nanjing, China). Mouse GPR39 (NP_081953.2) cDNA was cloned from the mouse pancreas. Human GPR39 (NP_001499.1) cDNA was purchased from Vigene Bio (Shandong, China). *G. Gallus* (NP_001073574.1), *G. japonicus* (XP_015264640.1), *X. laevis* (XP_041434441.1), and zebrafish (NP_956711.1) GPR39 cDNAs were synthesized by GenScript (Nanjing, China). All cDNAs were cloned into the pCMV6-Entry vector (OriGene), in which the GPCR was fused in frame with mCherry by a P2A linker. Site-directed mutagenesis to generate GPR39 mutants was carried out with the PCR overlap extension method, and all constructs were verified by sequencing.

Stable cell lines

Stable HEK293 cell lines expressing the mouse GPR39 gene were generated by the lentivirus system. Briefly, mouse GPR39 fused with mCherry by a P2A linker was cloned into the pLVX vector (Clontech). pLVX-mGPR39-P2A-mCherry plasmid was cotransfected with packaging plasmids pMD2.G (Addgene, 12259) and psPAX2 (Addgene, 12260) into HEK293T cells using Lipofectamine 3000 (Invitrogen). After 24 hours of transfection, the cells were treated with puromycin (2 μg/ml) for 2 days, before the selection of GPR39-expressing single clones by mCherry fluorescence protein using flow sorting. Stable human GPR39-expressing cell lines were obtained similarly.

Animals

GPR39-HA knock-in mice ($Gpr39^{HA}$) and GPR39 knockout mice ($Gpr39^{KO}$ or $Gpr39^{-/-}$) were created with CRISPR/EGE platform in the C57BL/6 strain by Beijing Biocytogen. For GPR39 knockout mice, the first 750 bps in exon 1 of the *Gpr39* gene was replaced by the iCreERT2-WPRE-PA element. All strains were verified by PCR sequencing of the targeted region, and Southern blots were performed to rule out random insertions. *Gpbar1* knockout mice ($Gpbar1^{-/-}$) in C57BL/6 background were donated by C. Jiang (*100*). All animal procedures performed in this paper were approved by the Institutional Animal Care and Use Committee of Peking University.

Ca^{2+} imaging

HEK293T cells were cultured in Dulbecco's minimum essential media (DMEM) supplemented with 10% fetal bovine serum (FBS) and 1% penicillin/streptomycin at 37°C and 5% CO_2. For preliminary screening of the 20 candidate GPCRs, HEK293T cells stably expressing $G_{\alpha 15}$ and GCaMP6s were used. HEK293T-$G_{\alpha 15}$-GCaMP6s cells were seeded in poly-D-lysine (PDL)–coated clear bottom 96-well plates. The next day, GPCR expressing constructs were transfected before replacement of the culture medium with 50 μl of recording buffer [150 mM NaCl, 4 mM KCl, 10 mM Hepes, 11 mM glucose, 2 mM $MgCl_2$, and 2 mM $CaCl_2$ (pH 7.4)] in each well 16 hours after transfection. A Leica TCS SP5 microscope was used to monitor intracellular Ca^{2+} changes induced by 50 μl of BA, which was added into the well by a pipette. If Fluo-8 AM (AAT Bioquest) was used, culture media were first replaced by 50 μl of dye loading buffer [Fluo-8 AM (2 μg/ml) in recording buffer] before incubation for 25 min at room temperature (RT). The dye loading buffer was replaced by an equal volume of recording buffer for 5 min before recording.

For Fluorescent Imaging Plate Reader (FLIPR) Ca^{2+} imaging assay, cells were seeded in PDL-coated 96-well plates. Dye loading and recording buffers were replaced as described above. Cells were imaged in the FLIPR at RT. The reading time interval of FLIPR was set as 1 s and 50 μl of the solution was dispensed into the plate at the 30th second, followed by 150 s of recording. If stable GPR39-expressing cell lines were used, we seeded the cells in PDL-coated 96-well plates directly the day before the experiment and ensured that cells reached a 90% density before imaging.

Measurement of GPBAR1 activation

Activation of GPBAR1 by BAs was detected by the CRE and luciferase reporter system (*63*). The GPBAR1-expressing reporter cell line was a gift from Y. Li. Briefly, when cells reached nearly 100% density in 96-well plates, the culture medium was replaced by FBS-free DMEM supplemented with indicated BAs. Cells were cultured at 37°C in 5% CO_2 for 10 hours. After which, 10 μl of the medium in each well was transferred into a 96-well plate, and 100 μl of coelenterazine-h solution [2.5 μg/ml in phosphate-buffered saline (PBS)] was added. After 2-min incubation, luminescence was detected by an EnVision plate reader. One hundred microliters of TLCA was used as the positive control, and the luminescence of TLCA-treated wells was set as 100% and the others were normalized.

Calculation of the RAi of receptors

The RAi values (*64*) were used to quantify the potency and the efficacy of BAs. For each receptor, the efficacy value (E_{max}) of each BA was divided by the EC_{50}, and the E_{max}/EC_{50} value was normalized to the maximum value among 30 BAs. We took the logarithm (Log_{10}) of the normalized E_{max}/EC_{50} to give a LogRAi value. To quantify BAs that have an ambiguous EC_{50} (EC_{50} > 100 μM or EC_{50} > 200 μM), we set these EC_{50} values as 200 μM. To obtain a converged LogRAi value, a normalized RAi value smaller than 0.001 was set as 0.001. For the GPR39 receptor, we calculated the RAi values in the presence or absence of 4 μM Zn^{2+} separately.

Immunostaining of mouse pancreases

Freshly isolated pancreases were fixed in 4% paraformaldehyde and dehydrated by 30% sucrose. Then, cryosections (40 μm) were cut

using a freezing microtome (Leica CM 3050). For detecting the expression of HA-tagged GPR39 in pancreas slides, rabbit anti-HA antibody (1:500 dilution; CST, catalog no. 3724S) was used, and the secondary antibody was Alexa Fluor 488 anti-rabbit immunoglobulin G (1:2000 dilution; Life Technology). Slides were mounted with DAPI Fluoromount-G (SouthernBiotech, catalog no. 0100-20) and imaged by a confocal microscope (Zeiss LSM880).

Acinar cell isolation and Ca^{2+} imaging

Acinar cells were prepared according to previous reports (*101*, *102*). Briefly, Hepes-buffered DMEM (Macklin, D6512) with SBTI (0.1 mg/ml; Sigma-Aldrich, T9128) bubbled with O_2 was used as the dissection buffer. The freshly dissected pancreas was digested with collagenase IV (2 mg/ml; Sigma-Aldrich, V900893) dissolved in the dissection buffer containing BSA (2.5 mg/ml). Five milliliters of collagenase solution was repeatedly injected into the pancreas before the pancreas was cut into small pieces and transferred into a flask. After gassing with O_2, the flask was incubated at 37°C with shacking at 120 rpm for 10 min, and then collagenase was replaced with 5 ml of fresh solution, and the pancreas was digested for another 30 min. The pieces were dissociated into acini by gently pipetting and the suspension was then filtered through 50-μm nylon cloth into a 50-ml centrifuge tube. Acini were further separated and collected from the suspension by centrifugation as described (*102*) and maintained in the dissection buffer containing BSA (1 mg/ml) before imaging. Cells were imaged in the acinus recording buffer [95 mM NaCl, 4.7 mM KCl, 20 mM Hepes, 10 mM glucose, 2 mM glutamine, 0.6 mM $MgCl_2$, 1.3 mM $CaCl_2$, and 1 × nonessential amino acids (pH at 7.4)]. Freshly isolated acinar cells were loaded with Fluo-8 AM (4 μg/ml) for 30 min at RT in the acinus recording buffer. Cells settled on a Cell-Tak (Corning) treated φ12-mm slide before the slide was placed in a perfusion chamber. Intracellular Ca^{2+} changes were monitored by a Zeiss LSM 710 microscope.

Cell death detection

Acini used in cell injury/death assay were isolated in a protocol slightly modified from what was described above. The concentration of collagenase IV solution was 1 mg/ml and 150-μm nylon cloth was used to collect larger acini. Isolated acini were resuspended in Hepes-buffered DMEM/F12 [with BSA (1 mg/ml)] (*103*) and distributed into a 48-well plate. Acini were incubated with test compounds at 37°C for 4 hours and LDH activities in the supernatant were quantified using an LDH cytotoxicity assay kit (Roche, 4744934001). Total LDH activities were measured after cells were lysed by 0.5% Triton X-100, and the LDH release was expressed as a percentage of the total LDH activity.

For PI uptake assay, acini were incubated with BAs for 4 hours at 37°C in a 48-well plate. After removing the supernatant gently, acini were resuspended in a medium containing PI (2 μg/ml). Then, 100 μl of the cell suspension was applied to a 384-well plate, and PI fluorescence was measured by a BioTek Cytation5 microplate reader (bottom reading mode; excitation, 536 nm; emission, 617 nm). PI fluorescence in the acini was normalized to that of vehicle control.

Amylase release detection

Acini used in amylase release detection were isolated and maintained in a protocol similar to that described for LDH leakage detection. Acini were incubated with BAs at 37°C for 30 min and the amylase activity in the supernatant was measured with an amylase activity assay kit (Sigma-Aldrich, MAK009). Amylase release of acini treated with the vehicle was measured as basal leakage and total amylase activity was measured after acini were lysed by 0.5% Triton X-100. The net amylase release was calculated by subtracting basal leakage in each group and expressed as a percentage of the total amylase activity.

Retrograde infusion of BA-induced acute pancreatitis models

Ten- to 12-week-old male mice (of 25 to 28 g in weight) were anesthetized with isoflurane. BA solution (or saline) containing methyl blue (1 mg/ml) was retrogradely infused into the pancreatic duct via a microsyringe pump at a flow rate of 5 μl/min for 10 min as described (*78*). TLCAS (5 mM) was used and dissolved in 0.9% NaCl solution. For LCAS, due to its poor solubility in 0.9% NaCl solution, 3 mM LCAS was used and dissolved in PBS (pH 7.4). All BA solutions should be freshly prepared to avoid precipitation. The severity of pancreatitis was monitored 24 hours after the induction. Serum was collected to determine the amylase and lipase levels using commercially supplied kits (Nanjing Jiancheng, C016 for amylase, A054 for lipase). For histopathology, a fresh pancreas colored with methyl blue was dissected and trimmed to a size of 5 mm by 5 mm. After sample fixation, paraffin sections were prepared and stained with hematoxylin and eosin, and scored blindly (edema grade as 0 = absent, 1 = focally increased between lobules, 2 = diffusely increased between lobules, 3 = acini disrupted, 4 = acini separated; inflammatory cell infiltration grade as 0 = absent, 1 = around ductal margins in ducts, 2 = in <20% of the lobules of the parenchyma, 3 = in 20 to 50% of the lobules of the parenchyma, 4 = in >50% of the lobules of the parenchyma; and acinar necrosis grade as 0 = absent, 1 = <5% periductal necrosis, 2 = 5 to 20% focal parenchymal necrosis, 3 = 20 to 50% diffuse parenchymal necrosis, 4 = > 50% diffuse parenchymal necrosis) according to previous reports with slight modifications (*104*, *105*).

Statistics

All statistical analyses were carried out with Prism 8 (GraphPad Software). Student's *t* test was used to compare two columns of data. One-way analysis of variance (ANOVA) followed by Tukey's multiple comparison posttest was used to compare multiple columns of data. Statistical significance is denoted by asterisks: n.s. $P > 0.05$, $*P < 0.05$, $**P < 0.01$, and $***P < 0.001$.

Supplementary Materials

This PDF file includes:

Figs. S1 to S8
Tables S1 and S2

REFERENCES AND NOTES

1. M. S. Petrov, D. Yadav, Global epidemiology and holistic prevention of pancreatitis. *Nat. Rev. Gastroenterol. Hepatol.* **16**, 175–184 (2019).
2. C. E. Forsmark, S. S. Vege, C. M. Wilcox, Acute pancreatitis. *N. Engl. J. Med.* **375**, 1972–1981 (2016).
3. C. Bernard, *Leçons de physiologie expérimentale appliquée à la médecine: Cours du semestre d'été. 2*. (Baillière, 1856).
4. E. L. Opie, The etiology of acute hemorrhagic pancreatitis. *Bull. Johns Hopkins Hosp.* **12**, 182–188 (1901).
5. W. S. Halsted, Retrojection of bile into the pancreas: A cause of acute hemorrhagic pancreatitis. *Bull. Johns Hopkins Hosp.* **12**, 179–182 (1901).
6. E. L. Opie, The relation of cholelithiasis to disease of the pancreas. *JAMA* **XLIII**, 1102–1105 (1904).

7. E. L. Opie, The relation OP cholelithiasis to disease of the pancreas and to fat necrosis. *Am. J. Med. Sci.* **121**, 27–42 (1901).
8. J. M. Acosta, C. L. Ledesma, Gallstone migration as a cause of acute pancreatitis. *N. Engl. J. Med.* **290**, 484–487 (1974).
9. A. Peracchia, M. Gafa, L. Sarli, M. Lupi, E. Longinotti, Biliary microlithiasis and acute pancreatitis. *Int. Surg.* **70**, 315–318 (1985).
10. E. Ros, S. Navarro, C. Bru, A. Garcia-Puges, R. Valderrama, Occult microlithiasis in 'idiopathic' acute pancreatitis: Prevention of relapses by cholecystectomy or ursodeoxycholic acid therapy. *Gastroenterology* **101**, 1701–1709 (1991).
11. S. P. Lee, J. F. Nicholls, H. Z. Park, Biliary sludge as a cause of acute pancreatitis. *N. Engl. J. Med.* **326**, 589–593 (1992).
12. P. Pallagi, T. Madacsy, A. Varga, J. Maleth, Intracellular Ca^{2+} signalling in the pathogenesis of acute pancreatitis: Recent advances and translational perspectives. *Int. J. Mol. Sci.* **21**, 4005 (2020).
13. Q. T. Tran, V. H. Tran, M. Sendler, J. Doller, M. Wiese, R. Bolsmann, A. Wilden, J. Glaubitz, J. M. Modenbach, F. G. Thiel, L. L. de Freitas Chama, F. U. Weiss, M. M. Lerch, A. A. Aghdassi, Role of bile acids and bile salts in acute pancreatitis: From the experimental to clinical studies. *Pancreas* **50**, 3–11 (2021).
14. A. Saluja, V. Dudeja, R. Dawra, R. P. Sah, Early intra-acinar events in pathogenesis of pancreatitis. *Gastroenterology* **156**, 1979–1993 (2019).
15. K. A. Muili, D. Wang, A. I. Orabi, S. Sarwar, Y. Luo, T. A. Javed, J. F. Eisses, S. M. Mahmood, S. Jin, V. P. Singh, M. Ananthanaravanan, G. Perides, J. A. Williams, J. D. Molkentin, S. Z. Husain, Bile acids induce pancreatic acinar cell injury and pancreatitis by activating calcineurin. *J. Biol. Chem.* **288**, 570–580 (2013).
16. K. A. Muili, S. Jin, A. I. Orabi, J. F. Eisses, T. A. Javed, T. Le, R. Bottino, T. Jayaraman, S. Z. Husain, Pancreatic acinar cell nuclear factor κB activation because of bile acid exposure is dependent on calcineurin. *J. Biol. Chem.* **288**, 21065–21073 (2013).
17. P. J. Lee, G. I. Papachristou, New insights into acute pancreatitis. *Nat. Rev. Gastroenterol. Hepatol.* **16**, 479–496 (2019).
18. A. Wahlstrom, S. I. Sayin, H. U. Marschall, F. Backhed, Intestinal crosstalk between bile acids and microbiota and its impact on host metabolism. *Cell Metab.* **24**, 41–50 (2016).
19. B. L. Copple, T. Li, Pharmacology of bile acid receptors: Evolution of bile acids from simple detergents to complex signaling molecules. *Pharmacol. Res.* **104**, 9–21 (2016).
20. A. F. Hofmann, L. R. Hagey, Key discoveries in bile acid chemistry and biology and their clinical applications: History of the last eight decades. *J. Lipid Res.* **55**, 1553–1595 (2014).
21. M. Makishima, T. T. Lu, W. Xie, G. K. Whitfield, H. Domoto, R. M. Evans, M. R. Haussler, D. J. Mangelsdorf, Vitamin D receptor as an intestinal bile acid sensor. *Science* **296**, 1313–1316 (2002).
22. M. Makishima, A. Y. Okamoto, J. J. Repa, H. Tu, R. M. Learned, A. Luk, M. V. Hull, K. D. Lustig, D. J. Mangelsdorf, B. Shan, Identification of a nuclear receptor for bile acids. *Science* **284**, 1362–1365 (1999).
23. D. J. Parks, S. G. Blanchard, R. K. Bledsoe, G. Chandra, T. G. Consler, S. A. Kliewer, J. B. Stimmel, T. M. Willson, A. M. Zavacki, D. D. Moore, J. M. Lehmann, Bile acids: Natural ligands for an orphan nuclear receptor. *Science* **284**, 1365–1368 (1999).
24. T. Maruyama, Y. Miyamoto, T. Nakamura, Y. Tamai, H. Okada, E. Sugiyama, T. Nakamura, H. Itadani, K. Tanaka, Identification of membrane-type receptor for bile acids (M-BAR). *Biochem. Biophys. Res. Commun.* **298**, 714–719 (2002).
25. Y. Kawamata, R. Fujii, M. Hosoya, M. Harada, H. Yoshida, M. Miwa, S. Fukusumi, Y. Habata, T. Itoh, Y. Shintani, S. Hinuma, Y. Fujisawa, M. Fujino, A G protein-coupled receptor responsive to bile acids. *J. Biol. Chem.* **278**, 9435–9440 (2003).
26. H. Wang, J. Chen, K. Hollister, L. C. Sowers, B. M. Forman, Endogenous bile acids are ligands for the nuclear receptor FXR/BAR. *Mol. Cell* **3**, 543–553 (1999).
27. C. Thomas, R. Pellicciari, M. Pruzanski, J. Auwerx, K. Schoonjans, Targeting bile-acid signalling for metabolic diseases. *Nat. Rev. Drug Discov.* **7**, 678–693 (2008).
28. A. Molinaro, A. Wahlstrom, H. U. Marschall, Role of bile acids in metabolic control. *Trends Endocrinol. Metab.* **29**, 31–41 (2018).
29. T. Q. de Aguiar Vallim, E. J. Tarling, P. A. Edwards, Pleiotropic roles of bile acids in metabolism. *Cell Metab.* **17**, 657–669 (2013).
30. C. Thomas, A. Gioiello, L. Noriega, A. Strehle, J. Oury, G. Rizzo, A. Macchiarulo, H. Yamamoto, C. Mataki, M. Pruzanski, R. Pellicciari, J. Auwerx, K. Schoonjans, TGR5-mediated bile acid sensing controls glucose homeostasis. *Cell Metab.* **10**, 167–177 (2009).
31. L. Adorini, M. Pruzanski, D. Shapiro, Farnesoid X receptor targeting to treat nonalcoholic steatohepatitis. *Drug Discov. Today* **17**, 988–997 (2012).
32. A. I. Orabi, K. A. Muili, T. A. Javed, S. Jin, T. Jayaraman, F. E. Lund, S. Z. Husain, Cluster of differentiation 38 (CD38) mediates bile acid-induced acinar cell injury and pancreatitis through cyclic ADP-ribose and intracellular calcium release. *J. Biol. Chem.* **288**, 27128–27137 (2013).
33. R. H. Palmer, The formation of bile acid sulfates: A new pathway of bile acid metabolism in humans. *Proc. Natl. Acad. Sci. U.S.A.* **58**, 1047–1050 (1967).
34. S. Voronina, R. Longbottom, R. Sutton, O. H. Petersen, A. Tepikin, Bile acids induce calcium signals in mouse pancreatic acinar cells: Implications for bile-induced pancreatic pathology. *J. Physiol.* **540**, 49–55 (2002).
35. J. Y. Kim, K. H. Kim, J. A. Lee, W. Namkung, A.-Q. Sun, M. Ananthanarayanan, F. J. Suchy, D. M. Shin, S. Muallem, M. G. Lee, Transporter-mediated bile acid uptake causes Ca^{2+}-dependent cell death in rat pancreatic acinar cells. *Gastroenterology* **122**, 1941–1953 (2002).
36. J. V. Gerasimenko, S. E. Flowerdew, S. G. Voronina, T. K. Sukhomlin, A. V. Tepikin, O. H. Petersen, O. V. Gerasimenko, Bile acids induce Ca^{2+} release from both the endoplasmic reticulum and acidic intracellular calcium stores through activation of inositol trisphosphate receptors and ryanodine receptors. *J. Biol. Chem.* **281**, 40154–40163 (2006).
37. G. Perides, J. M. Laukkarinen, G. Vassileva, M. L. Steer, Biliary acute pancreatitis in mice is mediated by the G-protein-coupled cell surface bile acid receptor Gpbar1. *Gastroenterology* **138**, 715–725 (2010).
38. S. G. Voronina, O. V. Gryshchenko, O. V. Gerasimenko, A. K. Green, O. H. Petersen, A. V. Tepikin, Bile acids induce a cationic current, depolarizing pancreatic acinar cells and increasing the intracellular Na^+ concentration. *J. Biol. Chem.* **280**, 1764–1770 (2005).
39. S. G. Voronina, S. L. Barrow, O. V. Gerasimenko, O. H. Petersen, A. V. Tepikin, Effects of secretagogues and bile acids on mitochondrial membrane potential of pancreatic acinar cells: Comparison of different modes of evaluating DeltaPsim. *J. Biol. Chem.* **279**, 27327–27338 (2004).
40. J. Louhimo, M. L. Steer, G. Perides, Necroptosis is an important severity determinant and potential therapeutic target in experimental severe pancreatitis. *Cell. Mol. Gastroenterol. Hepatol.* **2**, 519–535 (2016).
41. A. S. Hauser, M. M. Attwood, M. Rask-Andersen, H. B. Schioth, D. E. Gloriam, Trends in GPCR drug discovery: New agents, targets and indications. *Nat. Rev. Drug Discov.* **16**, 829–842 (2017).
42. A. P. Davenport, S. P. H. Alexander, J. L. Sharman, A. J. Pawson, H. E. Benson, A. E. Monaghan, W. C. Liew, C. P. Mpamhanga, T. I. Bonner, R. R. Neubig, J. P. Pin, M. Spedding, A. J. Harmar, International union of basic and clinical pharmacology. LXXXVIII. G protein-coupled receptor list: Recommendations for new pairings with cognate ligands. *Pharmacol. Rev.* **65**, 967–986 (2013).
43. S. M. Foord, T. I. Bonner, R. R. Neubig, E. M. Rosser, J. P. Pin, A. P. Davenport, M. Spedding, A. J. Harmar, International union of pharmacology. XLVI. G protein-coupled receptor list. *Pharmacol. Rev.* **57**, 279–288 (2005).
44. A. T. Ehrlich, G. Maroteaux, A. Robe, L. Venteo, M. T. Nasseef, L. C. van Kempen, N. Mechawar, G. Turecki, E. Darcq, B. L. Kieffer, Expression map of 78 brain-expressed mouse orphan GPCRs provides a translational resource for neuropsychiatric research. *Commun. Biol.* **1**, 102 (2018).
45. J. B. Regard, I. T. Sato, S. R. Coughlin, Anatomical profiling of G protein-coupled receptor expression. *Cell* **135**, 561–571 (2008).
46. S. P. Alexander, A. Christopoulos, A. P. Davenport, E. Kelly, N. V. Marrion, J. A. Peters, E. Faccenda, S. D. Harding, A. J. Pawson, J. L. Sharman, C. Southan, J. A. Davies; CGTP Collaborators, The concise guide to pharmacology 2017/18: G protein-coupled receptors. *Br. J. Pharmacol.* **174** (Suppl 1), S17–S129 (2017).
47. A. Wise, S. C. Jupe, S. Rees, The identification of ligands at orphan G-protein coupled receptors. *Annu. Rev. Pharmacol. Toxicol.* **44**, 43–66 (2004).
48. M. Rask-Andersen, S. Masuram, H. B. Schioth, The druggable genome: Evaluation of drug targets in clinical trials suggests major shifts in molecular class and indication. *Annu. Rev. Pharmacol. Toxicol.* **54**, 9–26 (2014).
49. K. Sriram, P. A. Insel, G protein-coupled receptors as targets for approved drugs: How many targets and how many drugs? *Mol. Pharmacol.* **93**, 251–258 (2018).
50. M. Kojima, K. Kangawa, Ghrelin: Structure and function. *Physiol. Rev.* **85**, 495–522 (2005).
51. K. L. Egerod, B. Holst, P. S. Petersen, J. B. Hansen, J. Mulder, T. Hokfelt, T. W. Schwartz, GPR39 splice variants versus antisense gene LYPD1: Expression and regulation in gastrointestinal tract, endocrine pancreas, liver, and white adipose tissue. *Mol. Endocrinol.* **21**, 1685–1698 (2007).
52. D. Moechars, I. Depoortere, B. Moreaux, B. de Smet, I. Goris, L. Hoskens, G. Daneels, S. Kass, L. Ver Donck, T. Peeters, B. Coulie, Altered gastrointestinal and metabolic function in the GPR39-obestatin receptor-knockout mouse. *Gastroenterology* **131**, 1131–1141 (2006).
53. L. Cohen, I. Sekler, M. Hershfinkel, The zinc sensing receptor, ZnR/GPR39, controls proliferation and differentiation of colonocytes and thereby tight junction formation in the colon. *Cell Death Dis.* **5**, e1307 (2014).
54. S. P. Meda Venkata, H. Li, L. Xu, J. Y. Koh, H. Nguyen, M. Minjares, C. Li, A. Kowluru, G. Milligan, J. M. Wang, Inhibition of GPR39 restores defects in endothelial cell-mediated neovascularization under the duress of chronic hyperglycemia: Evidence for regulatory roles of the sonic hedgehog signaling axis. *Proc. Natl. Acad. Sci. U.S.A.* **120**, e2208541120 (2023).
55. S.-I. Yasuda, T. Miyazaki, K. Munechika, M. Yamashita, Y. Ikeda, A. Kamizono, Isolation of Zn^{2+} as an endogenous agonist of GPR39 from fetal bovine serum. *J. Recept. Signal Transduct. Res.* **27**, 235–246 (2007).
56. B. Holst, N. D. Holliday, A. Bach, C. E. Elling, H. M. Cox, T. W. Schwartz, Common structural basis for constitutive activity of the ghrelin receptor family. *J. Biol. Chem.* **279**, 53806–53817 (2004).

57. B. Holst, K. L. Egerod, E. Schild, S. P. Vickers, S. Cheetham, L. O. Gerlach, L. Storjohann, C. E. Stidsen, R. Jones, A. G. Beck-Sickinger, T. W. Schwartz, GPR39 signaling is stimulated by zinc ions but not by obestatin. *Endocrinology* **148**, 13–20 (2007).
58. A. P. Campbell, A. V. Smrcka, Targeting G protein-coupled receptor signalling by blocking G proteins. *Nat. Rev. Drug Discov.* **17**, 789–803 (2018).
59. A. Segerstolpe, A. Palasantza, P. Eliasson, E. M. Andersson, A. C. Andreasson, X. Sun, S. Picelli, A. Sabirsh, M. Clausen, M. K. Bjursell, D. M. Smith, M. Kasper, C. Ammala, R. Sandberg, Single-cell transcriptome profiling of human pancreatic islets in health and type 2 diabetes. *Cell Metab.* **24**, 593–607 (2016).
60. T. M. Frimurer, F. Mende, A. S. Graae, M. S. Engelstoft, K. L. Egerod, R. Nygaard, L. O. Gerlach, J. B. Hansen, T. W. Schwartz, B. Holst, Model-based discovery of synthetic agonists for the Zn^{2+}-sensing G-protein-coupled receptor 39 (GPR39) reveals novel biological functions. *J. Med. Chem.* **60**, 886–898 (2017).
61. S. Peukert, R. Hughes, J. Nunez, G. He, Z. Yan, R. Jain, L. Llamas, S. Luchansky, A. Carlson, G. Liang, V. Kunjathoor, M. Pietropaolo, J. Shapiro, A. Castellana, X. Wu, A. Bose, Discovery of 2-pyridylpyrimidines as the first orally bioavailable GPR39 agonists. *ACS Med. Chem. Lett.* **5**, 1114–1118 (2014).
62. N. J. Alkayed, Z. Cao, Z. Y. Qian, S. Nagarajan, X. Liu, J. W. Nelson, F. Xie, B. Li, W. Fan, L. Liu, M. R. Grafe, C. M. Davis, X. Xiao, A. P. Barnes, S. Kaul, Control of coronary vascular resistance by eicosanoids via a novel GPCR. *Am. J. Physiol. Cell Physiol.* **322**, C1011–C1021 (2022).
63. H. Yu, T. Zhao, S. Liu, Q. Wu, O. Johnson, Z. Wu, Z. Zhuang, Y. Shi, L. Peng, R. He, Y. Yang, J. Sun, X. Wang, H. Xu, Z. Zeng, P. Zou, X. Lei, W. Luo, Y. Li, MRGPRX4 is a bile acid receptor for human cholestatic itch. *eLife* **8**, e48431 (2019).
64. A. Inoue, F. Raimondi, F. M. N. Kadji, G. Singh, T. Kishi, A. Uwamizu, Y. Ono, Y. Shinjo, S. Ishida, N. Arang, K. Kawakami, J. S. Gutkind, J. Aoki, R. B. Russell, Illuminating G-protein-coupling selectivity of GPCRs. *Cell* **177**, 1933–1947.e25 (2019).
65. H. Sato, A. Macchiarulo, C. Thomas, A. Gioiello, M. Une, A. F. Hofmann, R. Saladin, K. Schoonjans, R. Pellicciari, J. Auwerx, Novel potent and selective bile acid derivatives as TGR5 agonists: Biological screening, structure-activity relationships, and molecular modeling studies. *J. Med. Chem.* **51**, 1831–1841 (2008).
66. S. N. Chaudhari, D. A. Harris, H. Aliakbarian, J. N. Luo, M. T. Henke, R. Subramaniam, A. H. Vernon, A. Tavakkoli, E. G. Sheu, A. S. Devlin, Bariatric surgery reveals a gut-restricted TGR5 agonist with anti-diabetic effects. *Nat. Chem. Biol.* **17**, 20–29 (2021).
67. W. Alker, T. Schwerdtle, L. Schomburg, H. Haase, A Zinpyr-1-based fluorimetric microassay for free zinc in human serum. *Int. J. Mol. Sci.* **20**, 4006 (2019).
68. N. Barman, M. Salwa, D. Ghosh, M. W. Rahman, M. N. Uddin, M. A. Haque, Reference value for serum zinc level of adult population in bangladesh. *EJIFCC* **31**, 117–124 (2020).
69. L. Storjohann, B. Holst, T. W. Schwartz, Molecular mechanism of Zn^{2+} agonism in the extracellular domain of GPR39. *FEBS Lett.* **582**, 2583–2588 (2008).
70. A. F. Hofmann, L. R. Hagey, M. D. Krasowski, Bile salts of vertebrates: Structural variation and possible evolutionary significance. *J. Lipid Res.* **51**, 226–246 (2010).
71. M. Kojima, H. Hosoda, Y. Date, M. Nakazato, H. Matsuo, K. Kangawa, Ghrelin is a growth-hormone-releasing acylated peptide from stomach. *Nature* **402**, 656–660 (1999).
72. A. Moulin, L. Brunel, D. Boeglin, L. Demange, J. Ryan, C. M'Kadmi, S. Denoyelle, J. Martinez, J.-A. Fehrentz, The 1,2,4-triazole as a scaffold for the design of ghrelin receptor ligands: Development of JMV 2959, a potent antagonist. *Amino Acids* **44**, 301–314 (2013).
73. B. Holst, K. L. Egerod, C. Jin, P. S. Petersen, M. V. Østergaard, J. Hald, A. M. E. Sprinkel, J. Størling, T. Mandrup-Poulsen, J. J. Holst, P. Thams, C. Orskov, N. Wierup, F. Sundler, O. D. Madsen, T. W. Schwartz, G protein-coupled receptor 39 deficiency is associated with pancreatic islet dysfunction. *Endocrinology* **150**, 2577–2585 (2009).
74. C. K. Sung, J. A. Williams, Role of calcium in pancreatic acinar cell secretion. *Miner. Electrolyte Metab.* **14**, 71–77 (1988).
75. O. H. Petersen, R. Sutton, Ca^{2+} signalling and pancreatitis: Effects of alcohol, bile and coffee. *Trends Pharmacol. Sci.* **27**, 113–120 (2006).
76. S. Z. Husain, A. I. Orabi, K. A. Muili, Y. Luo, S. Sarwar, S. M. Mahmood, D. Wang, R. Choo-Wing, V. P. Singh, J. Parness, M. Ananthanaravanan, V. Bhandari, G. Perides, Ryanodine receptors contribute to bile acid-induced pathological calcium signaling and pancreatitis in mice. *Am. J. Physiol. Gastrointest. Liver Physiol.* **302**, G1423–G1433 (2012).
77. V. P. Singh, M. A. McNiven, Src-mediated cortactin phosphorylation regulates actin localization and injurious blebbing in acinar cells. *Mol. Biol. Cell* **19**, 2339–2347 (2008).
78. G. Perides, G. J. van Acker, J. M. Laukkarinen, M. L. Steer, Experimental acute biliary pancreatitis induced by retrograde infusion of bile acids into the mouse pancreatic duct. *Nat. Protoc.* **5**, 335–341 (2010).
79. J. M. Laukkarinen, G. J. D. Van Acker, E. R. Weiss, M. L. Steer, G. Perides, A mouse model of acute biliary pancreatitis induced by retrograde pancreatic duct infusion of Na-taurocholate. *Gut* **56**, 1590–1598 (2007).
80. K. K. McKee, C. P. Tan, O. C. Palyha, J. Liu, S. D. Feighner, D. L. Hreniuk, R. G. Smith, A. D. Howard, L. H. Van der Ploeg, Cloning and characterization of two human G protein-coupled receptor genes (GPR38 and GPR39) related to the growth hormone secretagogue and neurotensin receptors. *Genomics* **46**, 426–434 (1997).
81. J. V. Zhang, P.-G. Ren, O. Avsian-Kretchmer, C.-W. Luo, R. Rauch, C. Klein, A. J. W. Hsueh, Obestatin, a peptide encoded by the ghrelin gene, opposes ghrelin's effects on food intake. *Science* **310**, 996–999 (2005).
82. N. Chartrel, R. Alvear-Perez, J. Leprince, X. Iturrioz, A. Reaux-Le Goazigo, V. Audinot, P. Chomarat, F. Coge, O. Nosjean, M. Rodriguez, J. P. Galizzi, J. A. Boutin, H. Vaudry, C. Llorens-Cortes, Comment on "Obestatin, a peptide encoded by the ghrelin gene, opposes ghrelin's effects on food intake". *Science* **315**, 766 (2007).
83. E. Lauwers, B. Landuyt, L. Arckens, L. Schoofs, W. Luyten, Obestatin does not activate orphan G protein-coupled receptor GPR39. *Biochem. Biophys. Res. Commun.* **351**, 21–25 (2006).
84. E. T. van der Westhuizen, C. Valant, P. M. Sexton, A. Christopoulos, Endogenous allosteric modulators of G protein-coupled receptors. *J. Pharmacol. Exp. Ther.* **353**, 246–260 (2015).
85. A. S. Hauser, A. J. Kooistra, C. Munk, F. M. Heydenreich, D. B. Veprintsev, M. Bouvier, M. M. Babu, D. E. Gloriam, GPCR activation mechanisms across classes and macro/microscales. *Nat. Struct. Mol. Biol.* **28**, 879–888 (2021).
86. T. R. Ahmad, R. A. Haeusler, Bile acids in glucose metabolism and insulin signalling - mechanisms and research needs. *Nat. Rev. Endocrinol.* **15**, 701–712 (2019).
87. H. Azriel-Tamir, H. Sharir, B. Schwartz, M. Hershfinkel, Extracellular zinc triggers ERK-dependent activation of Na^+/H^+ exchange in colonocytes mediated by the zinc-sensing receptor. *J. Biol. Chem.* **279**, 51804–51816 (2004).
88. A. B. Podany, J. Wright, R. Lamendella, D. I. Soybel, S. L. Kelleher, ZnT2-mediated zinc import into Paneth cell granules is necessary for coordinated secretion and Paneth cell function in mice. *Cell. Mol. Gastroenterol. Hepatol.* **2**, 369–383 (2016).
89. Y. V. Li, Zinc and insulin in pancreatic beta-cells. *Endocrine* **45**, 178–189 (2014).
90. Y. Alnouti, Bile acid sulfation: A pathway of bile acid elimination and detoxification. *Toxicol. Sci.* **108**, 225–246 (2009).
91. S. P. Bathena, S. Mukherjee, M. Olivera, Y. Alnouti, The profile of bile acids and their sulfate metabolites in human urine and serum. *J. Chromatogr. B Analyt. Technol. Biomed. Life Sci.* **942-943**, 53–62 (2013).
92. R. Thakare, J. A. Alamoudi, N. Gautam, A. D. Rodrigues, Y. Alnouti, Species differences in bile acids II. bile acid metabolism. *J. Appl. Toxicol.* **38**, 1336–1352 (2018).
93. R. Thakare, J. A. Alamoudi, N. Gautam, A. D. Rodrigues, Y. Alnouti, Species differences in bile acids I. plasma and urine bile acid composition. *J. Appl. Toxicol.* **38**, 1323–1335 (2018).
94. I. M. Yousef, S. G. Barnwell, B. Tuchweber, A. Weber, C. C. Roy, Effect of complete sulfation of bile acids on bile formation in rats. *Hepatology* **7**, 535–542 (1987).
95. J. Huang, S. P. R. Bathena, I. L. Csanaky, Y. Alnouti, Simultaneous characterization of bile acids and their sulfate metabolites in mouse liver, plasma, bile, and urine using LC-MS/MS. *J. Pharm. Biomed. Anal.* **55**, 1111–1119 (2011).
96. M. Reich, C. Klindt, K. Deutschmann, L. Spomer, D. Haussinger, V. Keitel, Role of the G protein-coupled bile acid receptor TGR5 in liver damage. *Dig. Dis.* **35**, 235–240 (2017).
97. T. Li, J. Y. L. Chiang, Bile acid signaling in metabolic disease and drug therapy. *Pharmacol. Rev.* **66**, 948–983 (2014).
98. M. A. Hahn, C. Effertz, L. Bigler, E. von Elert, 5α-cyprinol sulfate, a bile salt from fish, induces diel vertical migration in *Daphnia*. *eLife* **8**, e44791 (2019).
99. M. Hahn, E. von Elert, L. Bigler, M. D. Diaz Hernandez, N. E. Schloerer, 5α-Cyprinol sulfate: Complete NMR assignment and revision of earlier published data, including the submission of a computer-readable assignment in NMReDATA format. *Magn. Reson. Chem.* **56**, 1201–1207 (2018).
100. X. Zheng, T. Chen, R. Jiang, A. Zhao, Q. Wu, J. Kuang, D. Sun, Z. Ren, M. Li, M. Zhao, S. Wang, Y. Bao, H. Li, C. Hu, B. Dong, D. Li, J. Wu, J. Xia, X. Wang, K. Lan, C. Rajani, G. Xie, A. Lu, W. Jia, C. Jiang, W. Jia, Hyocholic acid species improve glucose homeostasis through a distinct TGR5 and FXR signaling mechanism. *Cell Metab.* **33**, 791–803.e7 (2021).
101. A. I. Orabi, K. A. Muili, D. Wang, S. Jin, G. Perides, S. Z. Husain, Preparation of pancreatic acinar cells for the purpose of calcium imaging, cell injury measurements, and adenoviral infection. *J. Vis. Exp.*, e50391 (2013).
102. J. A. Williams, Isolation of rodent pancreatic acinar cells and acini by collagenase digestion. Pancreapedia: The Exocrine Pancreas Knowledge Base, (2010).
103. A. M. Reed, S. Z. Husain, E. Thrower, M. Alexandre, A. Shah, F. S. Gorelick, M. H. Nathanson, Low extracellular pH induces damage in the pancreatic acinar cell by enhancing calcium signaling. *J. Biol. Chem.* **286**, 1919–1926 (2011).
104. W. Du, G. Liu, N. Shi, D. Tang, P. E. Ferdek, M. A. Jakubowska, S. Liu, X. Zhu, J. Zhang, L. Yao, X. Sang, S. Zou, T. Liu, R. Mukherjee, D. N. Criddle, X. Zheng, Q. Xia, P. O. Berggren, W. Huang, R. Sutton, Y. Tian, W. Huang, X. Fu, A microRNA checkpoint for Ca^{2+} signaling and overload in acute pancreatitis. *Mol. Ther.* **30**, 1754–1774 (2022).
105. S. Wildi, J. Kleeff, J. Mayerle, A. Zimmermann, E. P. Bottinger, L. Wakefield, M. W. Buchler, H. Friess, M. Korc, Suppression of transforming growth factor β signalling aborts caerulein induced pancreatitis and eliminates restricted stimulation at high caerulein concentrations. *Gut* **56**, 685–692 (2007).

Acknowledgments: We are grateful to Y. Xian for the GPCR cDNA library; C. Jiang for sharing the GPBAR1 knockout mice; Y. Li for the CRE-nanoluciferase cell lines; S. Liu and W. Huang for help with

mouse AP models; Y. Zhao for help with Ca^{2+} signaling detection; the National Center for Protein Sciences at Peking University for access to instrumentation; the IMM Experimental Histopathology Platform at Peking University for assistance with paraffin sections and H&E staining; and Changping Laboratory, CLS, and CIBR for support. **Funding:** We are grateful to the Changping Laboratory and the Chinese Institutes for Medical Research for support. **Author contributions:** Conceptualization: Y.R. and Z.Z. Methodology: Y.R. and Z.Z. Investigation: Y.R. and Z.Z. Visualization: Z.Z. Supervision: Y.R. Writing—original draft: Z.Z. Writing—review and editing: Y.R. **Competing interests:** Z.Z. and Y.R. are coinventors of a pending international patent on the findings described here.

Data and materials availability: All data needed to evaluate the conclusions in the paper are present in the paper and/or the Supplementary Materials. Materials generated in this study are available from the corresponding author (Y.R.) upon reasonable request.

Submitted 2 June 2023
Accepted 4 January 2024
Published 2 February 2024
10.1126/sciadv.adj0146